

Intensity mapping with SDSS/BOSS Lyman- α emission, quasars and their Lyman- α forest.

Rupert A.C. Croft^{1*}, Jordi Miralda-Escudé^{2,3}, Zheng Zheng⁴, Michael Blomqvist⁵ and Matthew Pieri⁵

¹ *McWilliams Center for Cosmology, Dept. of Physics, Carnegie Mellon University, Pittsburgh, PA 15213, USA*

² *Institució Catalana de Recerca i Estudis Avançats, Barcelona, Catalonia*

³ *Institut de Ciències del Cosmos, Universitat de Barcelona/IEEC, Barcelona 08028, Catalonia*

⁴ *Department of Physics and Astronomy, University of Utah, 115 S 1400 E, Salt Lake City, UT 84112, USA*

⁵ *A*MIDEX, Aix Marseille Université, CNRS, LAM (Laboratoire d'Astrophysique de Marseille) UMR 7326, Marseille, France*

18 June 2018

ABSTRACT

We investigate the large-scale structure of Ly α emission intensity in the Universe at redshifts $z = 2 - 3.5$ using cross-correlation techniques. Our Ly α emission samples are spectra of BOSS Luminous Red Galaxies from Data Release 12 with the best fit model galaxies subtracted. We cross-correlate the residual flux in these spectra with BOSS quasars, and detect a positive signal on scales $1 \sim 15h^{-1}\text{Mpc}$. We identify and remove a source of contamination not previously accounted for, due to the effects of quasar clustering on cross-fibre light. Corrected, our quasar-Ly α emission cross-correlation is 50% lower than that seen by Croft et al. for DR10, but still significant. Because only $\sim 3\%$ of space is within $15h^{-1}\text{Mpc}$ of a quasar, the result does not fully explore the global large-scale structure of Ly α emission. To do this, we cross-correlate with the Ly α forest. We find no signal in this case. The 95% upper limit on the global Ly α mean surface brightness from Ly α emission-Ly α forest cross correlation is $\langle \mu_\alpha \rangle < 1.2 \times 10^{-22} \text{ erg s}^{-1} \text{ cm}^{-2} \text{ arcsec}^{-2}$. This null result rules out the scenario where the observed quasar-Ly α emission cross-correlation is primarily due to the large scale structure of star forming galaxies. Taken in combination, our results suggest that Ly α emitting galaxies contribute, but quasars dominate within $15h^{-1}\text{Mpc}$. A simple model for Ly α emission from quasars based on hydrodynamic simulations reproduces both the observed forest-Ly α emission and quasar-Ly α emission signals. The latter is also consistent with extrapolation of observations of fluorescent emission from smaller scales $r < 1h^{-1}\text{Mpc}$.

Key words: Cosmology: observations

1 INTRODUCTION

Intensity mapping (hereafter IM, Kovetz et al. 2016) refers to the use of one or more sharp spectral lines to directly trace out the large-scale structure of the Universe from the line emission intensity in the three-dimensional space of angular coordinates and redshift, without resolving discrete objects such as stars, galaxies or black holes. The technique has been studied most prominently in the case of 21cm emission from neutral hydrogen (e.g., Madau et al. 1997, Bandura et al. 2014), but theoretical predictions have been made for various strong atomic and molecular lines, including hydrogen Ly α (e.g., Pullen et al. 2014), CO (e.g., Carilli, 2011) and CII (e.g., Pullen et al. 2018). In the present paper we investigate Ly α intensity mapping, using spectra from the Sloan Digital Sky Survey

(SDSS, Eisenstein et al. 2011) and theoretical predictions using cosmological hydrodynamic simulations.

Observational measurements of structure using line intensity are most easily made using cross-correlation techniques, which avoids contamination by interloper lines (Pullen et al. 2016). This can be done when some other tracer of structure is available with a known redshift, such as galaxies or quasars in a redshift survey. The first three dimensional IM result (Chang et al. 2010) was obtained using 21cm data from the Green Bank telescope. A datacube of angular position and wavelength (converted into redshift using the 21cm rest wavelength) was cross-correlated with galaxy angular positions and redshifts from the DEEP2 galaxy catalogue (Davis et al. 2001). The resulting cross-correlation function of 21cm emission and galaxies was detected on scales from 1 to $20h^{-1}\text{Mpc}$. A tentative measurement using CII line emission has recently been made by Pullen et al. (2018), in cross-correlation with SDSS galaxies

* E-mail: rcroft@cmu.edu

and quasars. The CO Power Spectrum Survey (Keating et al. 2015) has also made a detection of fluctuations in CO emission, this time not using cross-correlation techniques, but a 3σ measurement of the bulk power spectrum. The final first detection we can mention at the present time is the quasar- $\text{Ly}\alpha$ cross-correlation presented by Croft et al (2016, hereafter C16) using both quasars and spectra from the SDSS tenth data release (DR10). In that case, a $\text{Ly}\alpha$ emission signal was seen within a separation of $15h^{-1}\text{Mpc}$ from quasars, but with an amplitude that was larger than expected from known $\text{Ly}\alpha$ emitters. In this paper we revisit $\text{Ly}\alpha$ IM using SDSS data, but this time we use DR12, which contains about 50% more spectra, and more importantly we use a new tracer for measuring the cross-correlation, the $\text{Ly}\alpha$ forest in absorption, alongside the quasars which were used before.

The hydrogen $\text{Ly}\alpha$ line has a long history as a probe of star formation in the high redshift Universe (Partridge & Peebles, 1967). Its strength and position in the observed frame visible spectrum when produced at the peak redshift for star formation has made it one of the prime candidates for IM (Pullen et al. 2014 and references therein). Reprocessed radiation from quasars or the UV background in general will also produce $\text{Ly}\alpha$ emission (e.g., Gould and Weinberg, 1996), and these components have been considered in IM predictions even at higher redshifts (Silva et al. 2013). Observations of discrete $\text{Ly}\alpha$ emitters from narrow band surveys and grism surveys, are now numerous (e.g., Wold et al. 2017) and have been used to constrain the star formation rate observable in $\text{Ly}\alpha$ emission (e.g., Gronwall et al. 2007), and clustering of the star forming galaxies responsible (e.g., Guaita et al. 2010). More extended $\text{Ly}\alpha$ emission has been seen as low surface brightness halos around $\text{Ly}\alpha$ emitting galaxies (Steidel et al. , 2011, Matsuda et al. , 2012, and Momose et al. , 2014), and the brightest extended objects have been seen proximate to quasars. These bright $\text{Ly}\alpha$ blobs (e.g., Cantalupo et al. 2014, Martin et al. 2014) have been studied using Integral Field Unit (IFU) spectroscopy, revealing structure in $\text{Ly}\alpha$ emission on scales up to a few hundred kpc from the central quasar.

Although IFUs have been used to study $\text{Ly}\alpha$ emission around quasars and galaxies (e.g., Gallego et al. 2018), the fields of view involved are small, a few arcseconds across. For large scale structure studies, large area spectral surveys are needed. There are several which are ongoing or upcoming, including HETDEX (Blanc et al. 2011), PAU (Castander et al. 2012), J-PAS (Benitez et al. 2014) and SPHEREx (Doré et al. 2014). Until the data is available, one can use data taken for other purposes to do IM. In C16 BOSS DR10 fibre spectra were used as $\text{Ly}\alpha$ emission samples, and in the present paper we will use BOSS DR12 (Alam et al. 2015). For cross-correlation one can use anything with a known redshift in the desired range. As $\text{Ly}\alpha$ is in the optical part of the spectrum at redshifts $z > 2$ the only large-area samples available for cross-correlation are quasars, and that is what was used in C16 and here (in the present case, the BOSS DR12 quasar sample, Pâris et al., 2017). Quasars do allow us to use another tracer of structure for cross-correlation, however, the $\text{Ly}\alpha$ forest. This has a low bias factor, leading to a lower signal in cross-correlation, but it has the advantage that it traces the intergalactic medium over a whole line of sight in every spectrum, and including all the volume of the Universe instead of the small fraction that is in the high density regions close to quasars.

As IM is carried out without identifying individual objects, contamination from other sources, such as interlopers at different redshift, light leakage, foreground or background emission is a difficult problem which all IM experiments will have to deal with. With 21cm IM, the Milky Way acts as an extremely strong source of foreground emission which is the limiting factor to current attempts to

apply IM to the epoch of reionization. Even with cross-correlation techniques it is easy for contamination to affect a potential signal, as was found in C16 (see appendices in that paper), where the cross-talk effect among spectra from fibres that are placed nearby in the BOSS camera implies that the $\text{Ly}\alpha$ emission light from quasars can pollute spectra in adjacent fibres used for $\text{Ly}\alpha$ detection, introducing artificial cross-correlations. These fibre pairs placed close to each other in the BOSS CCD camera were excluded from the cross-correlation, but as we shall see an effect due to quasar clustering that was neglected turns out to be important. In general, the subtleties of light contamination remain to be explored fully for precise measurements. One of the purposes of the present study is to reveal how contamination can enter and could be mitigated by properly designed dedicated IM experiments.

After dealing with contamination, C16 found the surprising result that there appears to be a high $\text{Ly}\alpha$ surface brightness around quasars at redshifts $z = 2 - 3.5$. It was deemed most likely that this was due to star forming galaxies, although this necessitated that most $\text{Ly}\alpha$ photons emitted by such galaxies are visible, but have not been detected by other means (perhaps due to an extremely low surface brightness). The other possibility was that the energy emanating from QSOs was the source of the $\text{Ly}\alpha$ emission instead. We will aim in this paper to decide between these two models, using a new dataset which includes the $\text{Ly}\alpha$ forest.

Whether quasars or galaxies are the source of the quasar- $\text{Ly}\alpha$ emission cross-correlation signal seen in C16, it is not clear whether a physical model can be constructed in the context of the large-scale distribution of matter and quasars predicted by the Cold Dark Matter model which is consistent with observations. We will set up some toy models based on cosmological hydrodynamic simulations to address this. There are many sophisticated models of $\text{Ly}\alpha$ emission and large-scale structure which use $\text{Ly}\alpha$ radiative transfer (e.g., Smith et al. 2018, Kakiichi & Djikstra 2017, Zheng et al. 2010, Kollmeier et al. 2010), but we will not be modeling the physical processes associated with $\text{Ly}\alpha$ emission, scattering and absorption. Instead we will "paint" a $\text{Ly}\alpha$ emission field onto the large-scale structure in the simulations and see whether it yields a quasar- $\text{Ly}\alpha$ emission cross-correlation and a $\text{Ly}\alpha$ emission- $\text{Ly}\alpha$ forest cross-correlation that are consistent with the measurements within the observational errors.

Our plan for the paper is as follows. In Section 2 we introduce the observational data we will be using, SDSS LRG spectra, quasars, and $\text{Ly}\alpha$ forest spectra. We compute the quasar- $\text{Ly}\alpha$ emission cross-correlation in Section 3 including comparison to the linear CDM model. We also measure the projected cross-correlation function and compare to an extrapolation of existing data on small scales. In Section 4 we focus on the $\text{Ly}\alpha$ forest- $\text{Ly}\alpha$ emission cross-correlation, attempting a measurement from SDSS data and using it to constraining the global $\text{Ly}\alpha$ surface brightness. In Section 5 we describe some toy models for the $\text{Ly}\alpha$ emission intensity based on cosmological hydrodynamic simulations and then compare them to our observational results. In Section 6 we summarize our findings and discuss their implications. In an Appendix, we show how we minimize light contamination in the measurements and test our methods with mock observations.

2 OBSERVATIONAL DATA

This study makes use of data from the SDSS BOSS survey Data Release 12 (DR12), including quasar position and redshift data, and galaxy and quasar spectra. The SDSS camera and telescope are

described in Gunn et al. (1998) and Gunn et al. (2006), respectively. Full information on the SDSS/BOSS spectrographs can be found in Smee et al. (2013). The wavelength coverage of the spectrograph is from $\lambda = 3560 \text{ \AA}$ to 10400 \AA the resolving power is $R \sim 1400$ for the range $\lambda = 3800 \text{ \AA} - 4900 \text{ \AA}$, and is kept above $R = 1000$ for the remainder of the wavelength range. The fibres have a diameter of $120 \mu\text{m}$, corresponding to 2 arcsec in angle. We restrict the redshift range of data we use in our analysis to $2.0 < z < 3.5$, due to the spectrograph cutoff at low redshift and the limited number of observed quasars at high redshift.

2.1 Quasar catalogue

For cross-correlation, we use quasars from the DR12 catalogue (P aris et al. 2017), which contains 297,301 spectroscopically confirmed quasars. The spectroscopic target selection procedure is that of Ross et al. (2012), which combines several algorithms to identify candidates, individually described in Richards et al. (2009); Kirkpatrick et al. (2011); Y eche et al. (2010); Bovy et al. (2011). The quasar redshifts have been obtained using the Principal Component Analysis method described in Paris et al. (2012), and Paris et al. (2017). We apply a quasar redshift cut, selecting only objects within the range $z = 2.0 - 3.5$. This reduces the number of quasars we use to 218726, with a mean redshift of $z = 2.55$.

2.2 Quasar Ly α forest spectra

We also use quasar Ly α forest spectra in our cross-correlation studies with Ly α emission. The quasar spectra in our sample are selected from the DR12 quasar catalogue. In order to avoid very short spectrum lengths, we use a slightly tighter cut of $z = 2.05 - 3.5$ than for the quasars in Section 2.1. The BAL quasars are discarded, as well as 3188 (very noisy) spectra which are flagged and removed by requiring a median S/N > 0 , normalisation factor > 0 , a minimum of 75 spectral pixels in the spectrum and a successful continuum fit (see below). These steps lead to a set of 161213 quasars in the forest sample.

We use the public DR13 pipeline reductions (Albareti et al., 2017) of the spectra, selecting the Ly α forest pixels which are in the restframe wavelength range of $1040 - 1200 \text{ \AA}$. We apply a minimum observed wavelength range of 3600 \AA and mask pixels affected by strong skylines based on the DR12 sky mask. We also mask DLAs and correct for the DLA wings, following the method described in Lee et al. (2013), using the catalogue of Noterdaeme et al. (2018)¹, (the method is described in Noterdaeme et al., 2009, 2012) to identify them. We fit the continuum to each spectrum using "method 1" of Busca et al. (2013) and (also known as "C1" by Delubac et al., 2015). To speed up the analysis we combine three adjacent spectral pixels into analysis pixels. The total number of these Ly α forest pixels used in our cross-correlation analyses is 22.92 million, and their mean redshift is $z = 2.41$.

2.3 Galaxy spectra

The 1570095 galaxy spectra in our sample are of targeted LRGs which are within redshifts $z \sim 0.15$ and $z \sim 0.7$ (mean redshift $z = 0.48$). In our study, as in C16, these galaxy spectra are used to measure Ly α emission, after a model spectrum of the targeted galaxy is subtracted from the observed spectrum. The redshift range

of the LRGs is not important for our purpose. For each spectrum, we make use only of the pixels for which the Ly α emission line is within the redshift range specified above ($2.0 < z < 3.5$). In observed wavelength this is from 3647 \AA to 5470 \AA .

The BOSS LRG program (Dawson et al. 2013) targeted two galaxy samples, CMASS ("constant mass") and LOWZ ("low-redshift"). The LOWZ galaxy sample is composed of massive red galaxies and spans $0.15 \lesssim z \lesssim 0.4$. The CMASS sample spans $0.4 \lesssim z \lesssim 0.7$.

The faintest galaxies are at $r = 19.5$ for LOWZ and $i = 19.9$ for CMASS. Both samples are color-selected to provide near-uniform sampling over the combined volume. Colors and magnitudes for galaxy selection are corrected for Galactic extinction using Schlegel et al. (1998) dust maps. We do not differentiate between the samples in our analysis.

The spectroscopic measurement pipeline for BOSS is described in detail in Bolton et al. (2012). The data products that are used in the present analysis are: (a) wavelength-calibrated, sky-subtracted, flux-calibrated, and co-added object spectra, which have been rebinned onto a uniform baseline of $\Delta \log_{10} \lambda = 10^{-4}$ (about $69 \text{ km s}^{-1} \text{ pixel}^{-1}$), (b) mask vectors for each spectrum, and (c) statistical error-estimate vectors for each spectrum (expressed as inverse variance) incorporating contributions from photon noise, CCD read noise, and sky-subtraction error.

2.4 Data preparation

Our Ly α emission samples are LRG spectra with the galaxy spectrum subtracted. The galaxy spectrum in each case is the best fit model provided by the pipeline. This template model spectrum (see Bolton et al. 2012 for details) is computed using least-squares minimization comparison of each galaxy spectrum to a full range of galaxy templates. Smooth terms absorb Galactic extinction, intrinsic extinction, and residual spectrophotometric calibration errors (typically at the 10% level) that are not fully spanned by the template basis sets. These basis sets are derived from restframe principal-component analyses (PCA) of training samples of galaxies.

After this subtraction, we compute the mean residual surface brightness per unit observed wavelength from all the spectra. We subtract this from each spectrum, as we are only interested in fluctuations in the Ly α emission surface brightness. This procedure is done as in C16, where it is describe in more detail. We also reject any pixels which fall within the mask for sky lines, as we have done with the Ly α forest spectra.

3 QUASAR-LYMAN-ALPHA EMISSION CROSS-CORRELATION

Before computing the quasar-Ly α emission cross-correlation, we first split the sample of galaxy and quasar spectra into 160 subsamples of approximately equal sky area based on contiguous groupings of plates. We then convert the galaxy spectrum pixels and the quasar angular positions and redshifts into comoving Cartesian coordinates using a flat cosmological model with matter density $\Omega_m = 0.315$, consistent with the Planck, Ade (2014) results (cosmological constant density $\Omega_\Lambda = 0.685$). This fiducial model is used throughout the paper.

We compute the quasar-Ly α emission surface brightness cross-correlation, $\xi_{q\alpha}(r)$, using a sum over all quasar-galaxy spectrum

¹ <http://www2.iap.fr/users/noterdae/DLA/DLA.html>

pixel pairs separated by r within a certain bin:

$$\xi_{q\alpha}(r) = \frac{1}{\sum_{i=1}^{N(r)} w_{ri}} \sum_{i=1}^{N(r)} w_{ri} \Delta_{\mu,ri}, \quad (1)$$

where $N(r)$ is the number of pixels in the bin centered on quasar-pixel distance r , and $\Delta_{\mu,ri} = \mu_{ri} - \langle \mu(z) \rangle$ is the residual surface brightness in the spectrum at pixel i for the bin r . Note here that we have a different list of pixels labeled as i for each bin in the separation r between a pixel and a quasar, which has Ly α surface brightness μ_{ri} . The residual flux at each pixel is obtained by subtracting the mean at each redshift, $\langle \mu(z) \rangle$. We weight each pixel by $w_{ri} = 1/\sigma_{ri}^2$, where σ_{ri}^2 is the pipeline estimate of the inverse variance of the flux at each pixel. We first present our results as a function of only the modulus of the quasar-pixel separation r in comoving h^{-1} Mpc, in 20 bins logarithmically spaced between $r = 0.5h^{-1}$ Mpc and $r = 150h^{-1}$ Mpc.

In C16 it was shown that stray light from the quasars themselves could contaminate the spectra of galaxies which are nearby on the spectrograph CCD. This occurs because the light from the various fibres is dispersed onto a single CCD, so that extraction of each spectrum along one dimension (Bolton et al. 2012) may include light from adjacent fibres on bright sources. Tests were carried out in C16 showing the presence of this stray light from quasars in galaxy spectra when the quasar and galaxy spectra were four fibres apart or fewer, in the list of fibres as they are ordered in the CCD. A constraint was applied so that galaxy and quasar spectra should be at least six fibres apart when computing the flux cross-correlation of equation 1. We have applied this restriction in this paper, both for the quasar-Ly α emission cross-correlation and for the Ly α forest-emission cross-correlation (presented later in Section 4).

In this paper, we have also carried out a further examination of systematic errors, and have found that this cross-fibre light can affect the results even when excluding close fibres from the cross-correlation. This is due to quasar clustering. Even when a specific quasar-galaxy pair is not used in the cross-correlation, light from other quasars spatially clustered with the first can contaminate nearby galaxy fibres. In Appendix A, we have tested three different methods for eliminating this contamination, which give statistically consistent results. Doing this involves removing all pixels which might be problematic from the dataset entirely (rather than just excluding certain pairs from the cross-correlation). This necessarily reduces the statistical power of the dataset. For example, removing all galaxy spectra which have a $z = 2.0 - 3.5$ quasar within ± 5 fibres reduces the number of galaxy spectra used from 1570095 to 37% of that number (574603). After accounting for the additional source of systematic error, we find a lower quasar-Ly α cross-correlation function amplitude (by a factor of approximately 2) compared to C16 (see Section 3.1 below for model fitting amplitude). For details of the cross-fibre light contamination, the reader is referred to Appendix A.

We use the 160 Jackknife samples to compute the mean of $\xi_{q\alpha}(r)$ and the error on the mean, as well as the covariance matrix of $\xi_{q\alpha}(r)$ (as in C16, Equation 7). In Figure 1 we show $\xi_{q\alpha}(r)$ for our fiducial sample (which is the entire dataset over the redshift range $2.0 < z < 3.5$). As in C16, the mean redshift of the sample is $z = 2.55$. We have removed the cross-fibre light contamination from the results using the pixel exclusion method from Appendix A. We can see from Figure 1 that there is evidence for an excess Ly α surface brightness within $r \approx 15h^{-1}$ Mpc of quasars, but not beyond this.

We also visually examine redshift space anisotropies in the

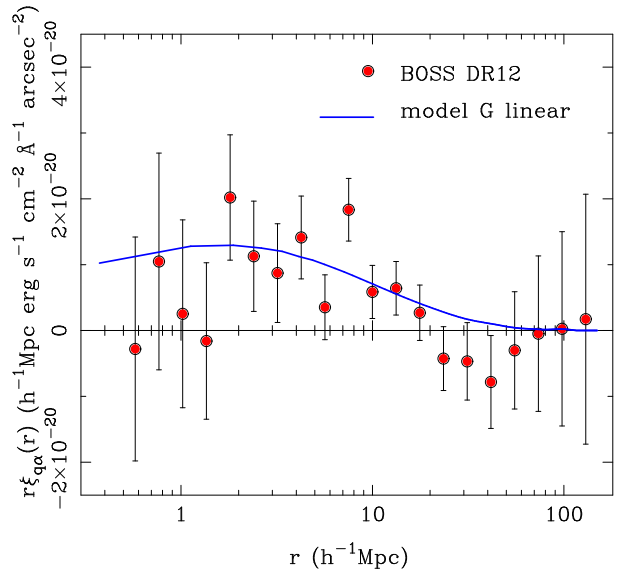


Figure 1. The quasar-Ly α emission cross-correlation function, $\xi_{q\alpha}(r)$ (see Equation 1). The points represent results for the fiducial sample that covers redshift range $2.0 < z < 3.5$. The error bars have been calculated using a jackknife estimator and 160 subsamples of the data. The smooth curve is a best fit linear CDM correlation function (see Section 3.1).

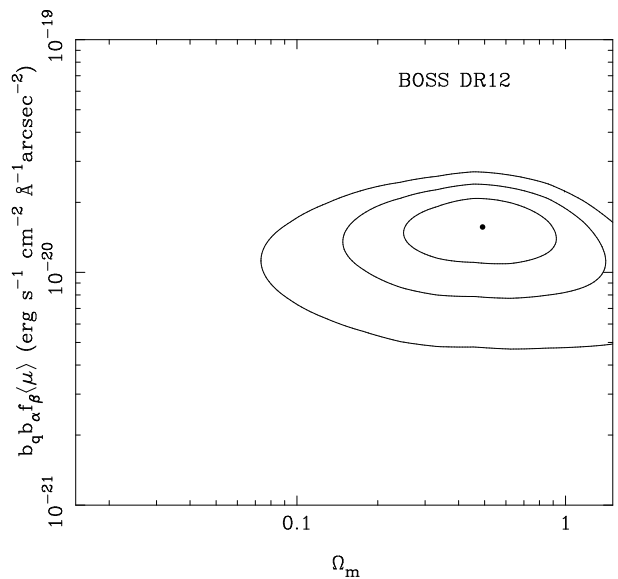


Figure 2. Fit parameters for the amplitude $b_q b_\alpha f_\beta \langle \mu \rangle$ and shape Ω_m (for fixed h and other parameters) of a linearly biased CDM model fit to the Ly α cross-correlation function plotted in Figure 1. The dot indicates the best fit parameters and the contours show the 1, 2 and 3 σ confidence contours.

correlation function $\xi_{q\alpha}$ by considering bins in the parallel and perpendicular components of r , r_{\parallel} and r_{\perp} . This is plotted in Figure 3. We can see that there appears to be some sign of visual elongation of the inner contours in the line of sight direction. In C16, the apparent signal to noise of the detection was large enough that we were able to make a measurement of this elongation, noting that it was consistent with that expected due to radiative transfer effects (Zheng et al., 2011). In the present work, due to the additional data cuts necessary to avoid all light contamination, the significance of

the signal is lower and we do not attempt to quantify any anisotropy, leaving this for future work with larger datasets.

3.1 Linear CDM fit: model G

In Figure 1, a solid curve is plotted. This is a Cold Dark Matter model fit. If the Ly α emission clustering is due to star forming galaxies tracing a linearly biased version of the density field, then a model for the isotropically averaged quasar-Ly α cross-correlation $\xi_{q\alpha}(r)$ is (see C16 for more details):

$$\xi_{q\alpha}(r) = b_q b_\alpha f_\beta \langle \mu_\alpha \rangle \xi(r) \quad (2)$$

where $\langle \mu_\alpha \rangle$ is the mean surface brightness of Ly α emission, b_q and b_α are the quasar and Ly α emission linear bias factors, $\xi(r)$ is the linear Λ CDM mass correlation function, and f_β is a constant enhancement to the correlation function on linear scales that is caused by peculiar velocity redshift-space distortions (Kaiser 1987). We refer to this model where galaxies are the source of Ly α emission as model G. Equation 2 represents the linear theory version of model G. In Section 5.1 we examine a version of model G based on simulations, as well as model Q, where quasars are responsible for the Ly α emission seen in the $\xi_{q\alpha}$ signal.

As in C16 we carry out a χ^2 fit for two free parameters in model G, the amplitude $b_q b_\alpha f_\beta \langle \mu \rangle$ and the shape, parametrised in the CDM power spectrum by Ω_m . In Figure 2 we show the best fit values of these parameters and their confidence contours. The best fit values and their one dimensional marginalized 1σ error intervals are

$$b_q b_\alpha f_\beta \langle \mu \rangle = 1.60_{-0.30}^{+0.32} \times 10^{-20} \text{ erg s}^{-1} \text{ cm}^{-2} \text{ arcsec}^{-2}, \quad (3)$$

and $\Omega_m = 0.491_{-0.174}^{+0.235}$. The shape, Ω is 1σ higher from the value obtained by C16, but the amplitude is lower by a factor of 2. These differences result from the removal of a newly discovered source of light contamination in the present work, due to (see Appendix A). Qualitatively, however, the conclusions drawn by C16 about $\xi_{q\alpha}$ remain applicable here: first that $\xi_{q\alpha}$ is consistent with the linear version of model G, but there is only clustering detected on scales smaller than $15h^{-1}\text{Mpc}$, and second that the amplitude in this model is much higher than would be expected if the Ly α emission detected were due to known Ly α emitters (see C16, Section 5 for a detailed treatment). We briefly recap here how these conclusions are reached.

In the context of this model (G), we take the amplitude $b_q b_\alpha f_\beta \langle \mu \rangle$ and use the published quasar bias value $b_q = 3.64_{-0.15}^{+0.13}$ (Font-Ribera et al. , 2013), and the $f_\beta = 0.8 \pm 0.15$ value from C16, to compute the mean Ly α surface brightness at $z = 2.55$, finding

$$\langle \mu_\alpha \rangle = (1.9 \pm 0.5) \times 10^{-21} (3/b_\alpha) \text{ erg s}^{-1} \text{ cm}^{-2} \text{ arcsec}^{-2}. \quad (4)$$

here b_α is the luminosity weighted bias factor of Ly α emission from star forming galaxies at $z = 2.55$, which C16 estimate should be $b_\alpha \sim 3$.

We convert this into a comoving Ly α luminosity density ϵ_α using

$$\epsilon_\alpha = 4\pi \langle \mu_\alpha \rangle \frac{H(z)}{c} \lambda_\alpha (1+z)^2, \quad (5)$$

where c is the speed of light and $\lambda_\alpha = 1216$. We find the value $\epsilon_\alpha = 1.5 \times 10^{41} (3/b_\alpha) \text{ erg s}^{-1} \text{ Mpc}^{-3}$. We then use the relationship $\text{SFR}/(M_\odot \text{ yr}^{-1}) = L_\alpha / (1.1 \times 10^{42} \text{ erg s}^{-1})$ (Cassata et al. 2011) to convert this into a measurement of the star formation rate density:

$$\rho_{\text{SFR}}(z = 2.55) = (0.14 \pm 0.04) \frac{3}{b_\alpha} M_\odot \text{ yr}^{-1} \text{ Mpc}^{-3}. \quad (6)$$

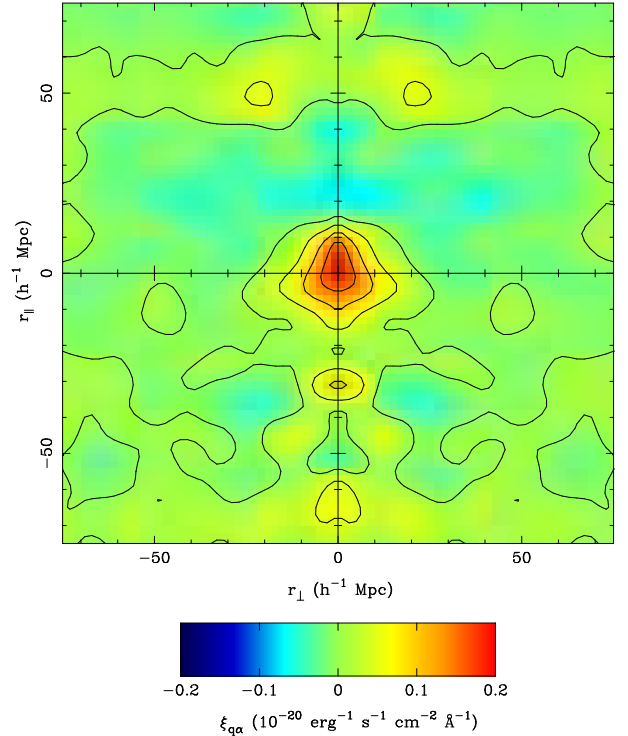


Figure 3. The quasar-Ly α cross-correlation $\xi_{q\alpha}$ as a function of r_{\parallel} and r_{\perp} . The units (of Ly α surface brightness) are the same as in Figure 1. The contours are spaced at values of $10^{-21} \text{ erg s}^{-1} \text{ cm}^{-2} \text{ arcsec}^{-2}$. To reduce noise in the image, the dataset was smoothed with a Gaussian filter with $\sigma = 4h^{-1}\text{Mpc}$ before plotting. Light contamination was excluded by using pixel veto (see Section 6.4 of Appendix A).

This value is 15 times higher (for $b_\alpha = 3$) than the Ly α emitter based measurements of Gronwall et al. (2007), Ouchi et al. (2008) or Cassata et al. (2011). As discussed in C16, this seems unlikely, but in absence of other constraints would be possible, as the extinction-corrected star formation rate density is similar to this value (Bouwens et al. , 2010). In the present paper, however we shall show that there are two pieces of evidence that model G with this high value of Ly α luminosity density does not apply to our Universe, but instead that quasars themselves are likely to be responsible for the $\xi_{q\alpha}$ signal. The first piece of evidence involves comparison with the Ly α emission seen around quasars on smaller scales, in the next Section.

3.2 Projected quasar-Lyman-alpha emission

In recent years, there have been several successful searches for Ly α emitting nebulae in close proximity to quasars. Cantalupo et al. (2014) and Hennawi et al. (2015) used custom narrow band filters to find two bright nebulae with diameters 460 proper kpc and 350 kpc respectively around quasars at redshifts $z \sim 2$. Martin et al. (2014) used the Cosmic Web Imager, an integral field spectrograph to detect extended emission around a large Ly α blob centered on a quasar. In these three cases the emission was consistent with quasar induced fluorescent emission (Hogan & Weymann 1987, Gould & Weinberg 1996, Cantalupo et al. 2005, Kollmeier et al. 2010). Although the detection rate with narrow band imaging was low (ten percent), a large IFU survey with the MUSE Spectrograph by Borisova et al. (2016) found that large Ly α nebulae appear to be ubiquitous around bright radio-quiet quasars, with 17 examples

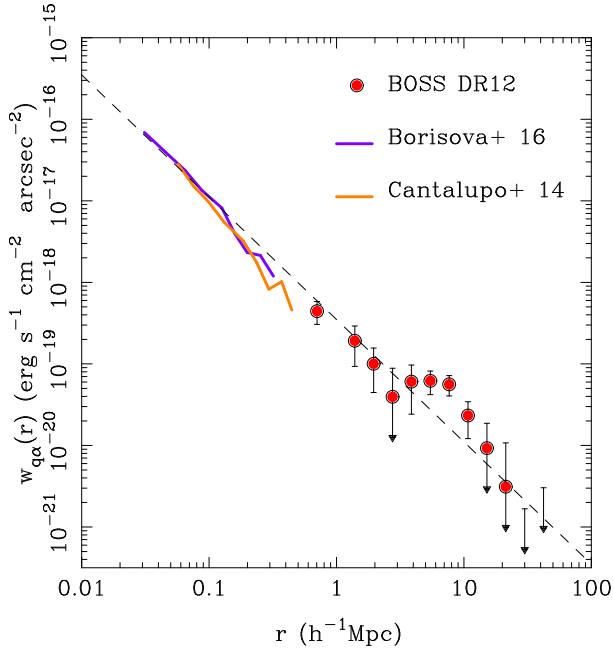


Figure 4. The projected quasar-Ly α emission cross-correlation function from BOSS compared to the small-scale results of Cantalupo et al. (2014) and Borisova et al. (2016). The BOSS results have been evaluated by projection into a pseudo narrow band with the same mean width as used by Borisova et al. (2016) (see text). The dashed line represents a power law $w_{q\alpha} = 3.5 \times 10^{-19} r^{-1.5} \text{ erg s}^{-1} \text{ cm}^{-2} \text{ arcsec}^{-2}$.

found. These observations were stacked by Borisova et al., yielding the circularly averaged surface brightness profile around quasars.

In Figure 4, we show the Borisova mean Ly α profile, as well as the circularly averaged Ly α surface brightness profile of the “Slug” nebula (Cantalupo et al. 2014). We have used $(1+z)^4$ surface brightness dimming to convert the Cantalupo et al. and Borisova et al. results to what they would be at the mean redshift of our present measurement ($z = 2.5$). In order to compare to our measurement of $\xi_{q\alpha}$ we project our results to account for the fact that the IFU observations have been projected into a pseudo narrow band. Borisova et al. fix the width of their pseudo-NB images to the maximum spectral width of the nebulae. These vary from 105 Å to 23.75 Å, with a mean width of 43.02 Å. This mean filter width translates to a comoving line of sight distance of $r_{\text{NB}} = 20.75 h^{-1} \text{ Mpc}$. We therefore take the $\xi_{q\alpha}(r_{\parallel}, r_{\perp})$ measurement shown in Figure 3 and collapse the region between $r_{\parallel} = \pm 20.75/2 h^{-1} \text{ Mpc}$ along the r_{\parallel} axis and plot the result as a function of r_{\perp} . We label the result w_{qe} , and show it in Figure 4, along with the Cantalupo et al. and Borisova et al. results.

We can see from Figure 4 that although there is not coincidence in spatial scales between the SDSS and IFU measurements, the scales are almost overlapping. The largest scale datapoint for the IFU data is at $0.4 h^{-1} \text{ Mpc}$, and the smallest SDSS point is at $0.7 h^{-1} \text{ Mpc}$. An extrapolation of the small scale IFU data appears to be reasonably consistent with the SDSS $w_{qe}(r)$. In order to guide the eye, we plot a power law $w(qe) = 3.5 \times 10^{-19} r^{-1.5} \text{ erg s}^{-1} \text{ cm}^{-2} \text{ arcsec}^{-2}$. This curve has no physical significance but appears to follow the broad trend seen in the data. This power law in Ly α surface brightness, seen over three orders of magnitude in spatial scale may indicate that the physical process or at least the quasar energetic output responsible for the small scale emission profile seen continues to act detectably $10 h^{-1} \text{ Mpc}$ from quasars.

4 LYMAN-ALPHA FOREST-LYMAN-ALPHA EMISSION CROSS-CORRELATION

If the Ly α emission seen in Section 3 were uniformly tracing the large-scale structure of the Universe, one would expect there to be significant Ly α surface brightness in regions that are far from quasars. The quasar-Ly α cross-correlation function is not the best way to probe this, due to the fact that the $\xi_{q\alpha}$ measurement is below the noise level at large quasar-pixel separations. In Figure 1 we can see that this occurs at scales $r \geq 15 h^{-1} \text{ Mpc}$. The luminosity function of SDSS quasars at redshift $z \approx 2.5$ is $\Phi = 10^{-5.8} \text{ Mpc}^{-3} \text{ mag}^{-1}$ at the $i = 21.8$ limit of the survey (DR9, Ross et al. 2013). The mean interquasar separation is approximately $50 h^{-1} \text{ Mpc}$. The volume fraction of space sampled by quasars is therefore $(15/50)^3 = 0.03$, and should be supplemented by a more space-filling tracer of Ly α emission to truly test whether the Ly α emission seen in Figure 1 is due to star forming galaxies.

The Ly α forest of absorption by neutral hydrogen in quasar spectra offers an alternative. The Ly α forest has long been used as a probe of the cosmic density field at the relevant redshifts. The physical processes governing the state of the IGM are simple, and its absorption properties are those first described by Gunn and Peterson (1965), leading to its characterization as the “Fluctuating Gunn-Peterson Effect” (Weinberg et al. 1997). On scales larger than a pressure smoothing scale (of order $0.1 h^{-1} \text{ Mpc}$, Peeples et al. 2010), the forest acts as a biased tracer of the density field. When dealing with Ly α forest clustering it is customary to define the “flux overdensity”, δ_F , from the observed flux “F” in a spectrum as follows:

$$\delta_F = \frac{F}{\langle F \rangle} - 1. \quad (7)$$

δ_F is a quantity with zero mean. On large scales, the quantity δ_F is related to the mean overdensity of matter by linear bias factor b_f . Because the Ly α forest is saturated in regions of high density, the clustering of the forest has a relatively low amplitude, and therefore a low bias factor. McDonald (2003) carried out a determination of the bias factor expected in CDM models, finding $b = -0.1511$. This is approximately consistent with e.g., the measurements of the Ly α forest autocorrelation function by Slosar et al. (2011), which yield $b = -0.2 \pm 0.02$. Because the quasar flux in a Ly α forest spectrum is absorbed more (lower flux) in regions of low density and is absorbed less (higher flux) in regions of high density, the relationship between δ_F and δ , the matter overdensity has a negative bias factor, b_f . This can be seen in various contexts, such as the negative cross-correlation function of quasars and the Ly α forest (Font-Ribera et al. 2014). The amplitude of the Ly α forest-emission correlation is therefore expected to be negative in models where high overdensities of matter (and Ly α emission) lead to increased Ly α absorption.

The forest has been used in a variety of cosmological measurements, including the determination of the Baryon Acoustic Oscillation scale from Ly α forest clustering at high redshifts (Busca et al. 2013, Slosar et al. 2013). In our case we will use it to probe cosmic Ly α emission using cross-correlation. In SDSS DR12, the number of high redshift $z > 2.15$ quasar spectra is 175244 over 9376 square degrees of spectroscopic effective area. This leads to a mean sightline separation of comoving $\sim 17 h^{-1} \text{ Mpc}$. This relatively high density of sightlines makes it possible to reconstruct the large-scale structure of the cosmic density field at these redshifts with higher resolution than is possible with current galaxy or quasar surveys (e.g., Ozbek and Croft 2016). The cross-correlation function of the

Ly α forest and Ly α emission, $\xi_{f\alpha}$ will therefore also be much better sampled, with many more Ly α forest- Ly α emission pixel pairs at any separation than was the case with $\xi_{q\alpha}$.

We compute $\xi_{f\alpha}$ from our data samples in a similar fashion to the quasar-Ly α emission cross correlation (Equation 1). Our estimator is

$$\xi_{fe}(r) = \frac{1}{\sum_{i=1}^{N(r)} w_{ri}} \sum_{i=1}^{N(r)} w_{ri} \Delta\mu \delta_F, \quad (8)$$

where δ_F is the Ly α forest flux overdensity.

We use the same 160 subvolumes of the survey to construct jackknife samples, and use these to compute errors bars as was done with $\xi_{q\alpha}$. As with $\xi_{q\alpha}$, we have found that there is some cross-fibre light which could affect the measurement. We again do not use pairs of Ly α forest and Ly α emission pixels which are separated by 5 fibres or less in computing Equation 8. After doing this, again as with $\xi_{q\alpha}$, a small amount of residual light contamination remains due to quasar clustering. This can be removed either by subtracting a model for the contamination or by completely removing all fibres with $\delta_{\text{fibre}} \leq 5$ from the sample. In Appendix A we carry out tests on both of these methods, and show that there is no significant difference in our conclusions when either is used, or even if the contamination is not corrected for (it is very small in the case of $\xi_{f\alpha}$).

In Figure 5 we show our results (in this case the modelled contamination has been subtracted). We can see that there does not appear to be any strong evidence for a non-zero $\xi_{f\alpha}$ signal. We will see later that a model fit shows that this is indeed a null result. Comparing Figure 5 to Figure 1, the y-axis scale has been magnified by a factor of 10, so that the overall signal in the quasar-emission correlation would be completely off the top of the panel in the current plot. Because the bias factor of the forest is much lower, however, one would expect the $\xi_{f\alpha}$ signal to be much smaller than $\xi_{q\alpha}$. We now examine this expectation in the context of the model where the Ly α emission surface brightness traces the large-scale structure of the Universe.

We have seen in Section 3.1 that if the $\xi_{q\alpha}$ signal seen is due to star forming galaxies which trace structure, then a very high mean Ly α surface brightness of $\langle\mu_\alpha\rangle = (1.9 \pm 0.5) \times 10^{-21} (3/b_\alpha) \text{ erg s}^{-1} \text{ cm}^{-2} \text{ arcsec}^{-2}$ is inferred, and this Ly α emission is associated with a star formation rate $\rho_{\text{SFR}}(z = 2.55) = (0.14 \pm 0.04) (3/b_\alpha) M_\odot \text{ yr}^{-1} \text{ Mpc}^{-3}$. In C16, a qualitatively similar conclusion was reached (although the results were approximately a factor of two higher due to the presence of contamination from quasar clustering). We are now in a position to test this model, as it predicts that for $\xi_{f\alpha}$ we should see the same shape as $\xi_{q\alpha}$ from Figure 1, but with the amplitude scaled down by a factor of $(-0.3/3.6)$, which is the ratio of the Ly α forest bias factor to the quasar bias factor. This value of -0.3 for the forest bias factor is approximate (see Slosar et al 2011), and includes the effect of redshift space distortions ($b_{f\beta} = -0.3$, see Section 4.1). Quasar redshift distortions have a negligible effect on the clustering amplitude in this context. We have plotted this prediction as a dot-dashed line in Figure 5. We can immediately see that it is not consistent with the DR12 results, which indicates that the Ly α emission seen in $\xi_{q\alpha}$ cannot be spread throughout space with a high surface brightness.

The other solid line in Figure 5 shows the predicted $\xi_{f\alpha}$ curve that corresponds to the same model, but with a much lower mean surface brightness of Ly α emission, that due to the summed emission of known Ly α emitters. The results of Gronwall et al. (2007)

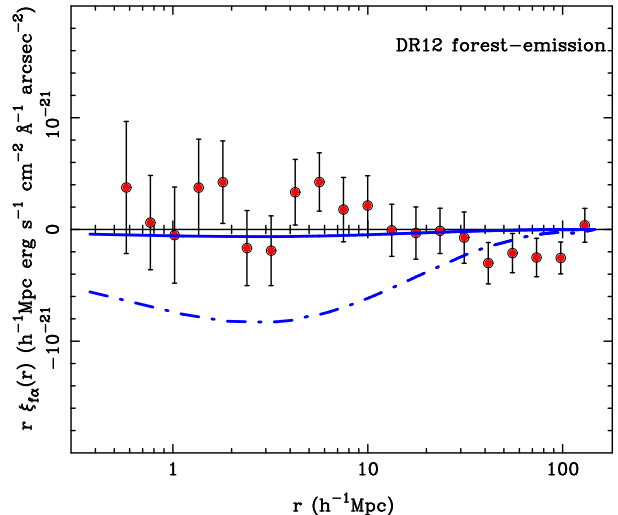


Figure 5. The cross-correlation function of Ly α emission and the Ly α forest, $\xi_{f\alpha}$ for spectra from BOSS DR12 (points with error bars) as a function of Ly α emission - Ly α forest pixel pair separation. The solid line shows the predicted cross-correlation function if the Ly α emission were tracing the large-scale structure of the Universe (for example being caused by star forming galaxies), and the mean surface brightness of Ly α emission in the Universe is given by the contribution of all individually detected Ly α emitters. It should be noted that the predicted amplitude of $\xi_{f\alpha}$ is negative (because the Ly α forest has negative bias). The dashed line shows the predicted cross-correlation function if the Ly α emission were tracing the large-scale structure of the Universe but the mean surface brightness of Ly α emission was at the very high level needed to account for the results in G. This is clearly ruled out, indicating that the mean surface brightness of Ly α emission must be at a lower level.

have shown that these correspond to a star formation rate at $z \sim 2.5$ observed through Ly α of $\rho_{\text{SFR}} = 0.01 M_\odot \text{ yr}^{-1}$. This is a factor of ~ 15 smaller than the high surface brightness model. By eye, it is apparent that this very low amplitude curve is not very different from zero given the error bars of the DR12 result. As such, the observed Ly α forest-Ly α emission cross-correlation appears to be consistent with known Ly α emitters. It is however possible to use $\xi_{f\alpha}$ to place limits on the presence of other Ly α emission that traces cosmic structure, including very low surface brightness emission that would not have been detected in Ly α emitter surveys.

4.1 Linear CDM fit to forest-emission cross-correlation: model G

We do this by carrying out model fitting, using the same biased linear CDM correlation function used in Section 3.1 (model G). The amplitude parameter in the present case is $b_f b_\alpha f_\beta \langle\mu\rangle$, and the shape parameter is again Ω_m . In figure 6 we show the contours of $\Delta\chi^2$ in this parameter space. We can see that the best fit model has a positive amplitude (the opposite sign to that expected for $\xi_{f\alpha}$), but that it is consistent with zero at the $\sim 1\sigma$ level, as we expected given our visual impression of Figure 5. The best fit parameters are

$$b_f b_\alpha f_\beta \langle\mu\rangle = (2.5 \pm 1.8) \times 10^{-22} \text{ erg s}^{-1} \text{ cm}^{-2} \text{ arcsec}^{-2}, \quad (9)$$

and $\Omega_m = 0.691^{+2.06}_{-0.47}$. In Figure 6 we have plotted symbols representing the high surface brightness Ly α model, and the Ly α model representing known Ly α emitters. The former lies at a $\Delta\chi^2 = 56.5$ from the best fit, indicating that it is ruled out at the 7.5σ level. The latter is within $\Delta\chi^2 = 3.7$ of the best fit, indicating that it

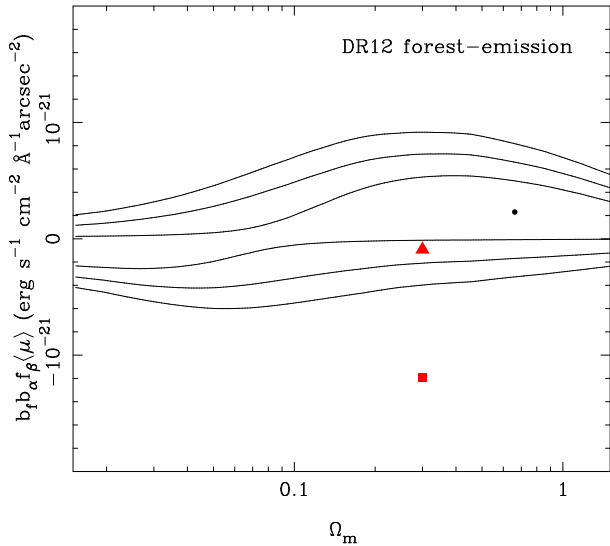


Figure 6. Fit parameters for the amplitude $b_f b_\alpha f_\beta(\mu)$ and shape Ω_m (for fixed h and other parameters) of a linearly biased CDM model fit to the forest- $\text{Ly}\alpha$ emission cross-correlation function plotted in Figure 5. The dot indicates the best fit parameters and the contours show the 1, 2 and 3 σ confidence contours. The triangle corresponds to the parameters for the solid theory line in Figure 5 (mean $\text{Ly}\alpha$ emission consistent with known $\text{Ly}\alpha$ emitters) and the square the dot-dashed theory line in Figure 5 (mean $\text{Ly}\alpha$ emission consistent with emission tracing large-scale structure, model G and an amplitude needed to fit the $\xi_{q\alpha}$ observations in this model). This model is clearly ruled out.

is acceptable at the 1.9σ level. Assuming a fixed shape parameter of $\Omega_m = 0.3$ leads to a 95 per cent lower limit on the parameter $b_f b_\alpha f_\beta(\mu) = -1.07 \times 10^{-22} \text{ erg s}^{-1} \text{ cm}^{-2} \text{ arcsec}^{-2}$. The 95 per cent upper limit on the mean $\text{Ly}\alpha$ surface brightness is then

$$\langle \mu_\alpha \rangle < 1.2 \times 10^{-22} \frac{-0.3}{b_f f_\beta} (3/b_\alpha) \text{ erg s}^{-1} \text{ cm}^{-2} \text{ arcsec}^{-2}. \quad (10)$$

Here we assume fiducial values of $b_f f_\beta = -0.3$ (motivated by Slosar et al. 2011) and $b_\alpha = 3$. This limit is in the context of model G, and is a factor of 15 lower than the value estimated from $\xi_{q\alpha}$ in Equation 5. The 95 per cent upper limit on the associated star formation rate density is therefore also a factor of 15 lower, and just consistent with the measurement from known $\text{Ly}\alpha$ emitters.

In order to confirm this null result, we can also examine $\xi_{f\alpha}$ as a function of pixel separation across and along the line of sight. This is shown in Figure 7. The expected signal in the event of significant $\text{Ly}\alpha$ forest- emission cross correlation would be negative, i.e. on the blue end of the colour table. We can see that instead the plot is mostly green, indicating no signal. Any hint of a positive correlation in the radially averaged version of this plot (Figure 1) is seen here to result from a faint blob which is off center, this fact, and the $\sim 1\sigma$ significance both point to their being an absence of signal.

There is therefore little room for excess surface brightness over that contributed by known $\text{Ly}\alpha$ emitters in this model of $\text{Ly}\alpha$ emission tracing large-scale structure. The question still remains whether there is a way that $\text{Ly}\alpha$ emission can be spatially distributed in a fashion which is consistent with both the $\xi_{q\alpha}$ and $\xi_{f\alpha}$ constraints. In order to address this we have carried out some simple theoretical modelling using a cosmological hydrodynamic simulation, as described in the next section.

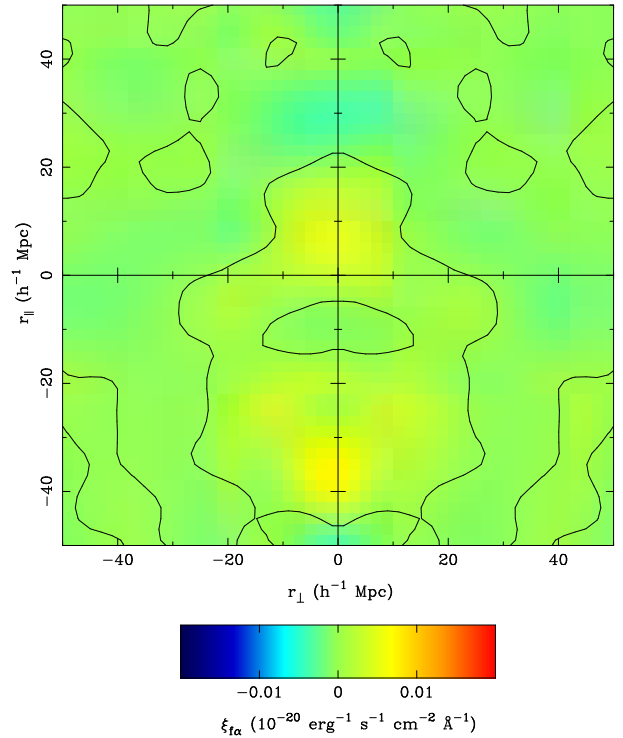


Figure 7. The cross-correlation function of $\text{Ly}\alpha$ emission and the $\text{Ly}\alpha$ forest, $\xi_{f\alpha}$ for spectra from BOSS DR12 (points with error bars) as a function of separation parallel to and perpendicular to the line of sight. The predicted amplitude of $\xi_{f\alpha}$ is negative (because the $\text{Ly}\alpha$ forest has negative bias). The cross-correlation function plotted here is consistent with noise.

5 COMPARISON TO SIMULATIONS

The $\text{Ly}\alpha$ surface brightness seen within $15 h^{-1} \text{ Mpc}$ of quasars is certainly substantial (Figure 1). We would like to know whether it is possible to model such a high surface brightness and yet not breach the $\xi_{f\alpha}$ constraint on $\text{Ly}\alpha$ emission from the more widely distributed intergalactic medium. To answer this, we set up some simple toy models using a cosmological simulation as a base.

5.1 Simulation model

In order to resolve the relevant pressure smoothing scale in the forest and large-scale structure, we use a large hydrodynamic cosmological simulation of the ΛCDM model. The smoothed particle hydrodynamics code P-GADGET (see Springel 2005, Di Matteo et al. 2012) was used to evolve $2 \times 4096^2 = 137$ billion particles in a cubical periodic volume of side length $400 h^{-1} \text{ Mpc}$. This simulation was previously used in Cisewski et al. (2014) and Ozbek and Croft (2016), where more details are given.

The simulation cosmological parameters were $h = 0.702$, $\Omega_\Lambda = 0.725$, $\Omega_m = 0.275$, $\Omega_b = 0.046$, $n_s = 0.968$ and $\sigma_8 = 0.82$. The mass per particle was $1.19 \times 10^7 h^{-1} M_\odot$ (gas) and $5.92 \times 10^7 h^{-1} M_\odot$ (dark matter). An ultraviolet background radiation field consistent with Haardt and Madau (1995) is included, as well as cooling and star formation. The latter, however uses a lower density threshold than usual (for example in Springel & Hernquist 2003) so that gas particles are rapidly converted to collisionless gas particles. This is done to speed up execution of the simulation. As a result the stellar properties of galaxies in the simulation are not predicted reliably but this has no significant effect

on the diffuse IGM that gives rise to the Lyman- α forest. We do not otherwise use the galaxies in our modeling, but instead use the overall baryonic density field to generate a biased Ly α emission spatial distribution (see below).

The simulation snapshot at redshift $z = 2.5$ (the mean redshift of our SDSS observations) is used to generate a set of Lyman- α spectra using information from the particle distribution (Hernquist et al. 1996). The spectra are generated on a grid with $256^2 = 65536$ evenly spaced sightlines, resulting in $1.56 h^{-1}$ Mpc spacing. We also use the simulation particles to generate a baryonic matter density field sampled along the same sightlines. This field will be used to model the Ly α emission.

We also use the baryonic matter density to generate quasars. To do this, we resample each sightline so that it has 256 pixels (the density field is now a 256^3 grid). We find all the local maxima in that grid and select the 512 with the highest local density to be the locations of quasars in our model. The mean quasar separation is therefore $50 h^{-1}$ Mpc, approximately consistent with the mean separation in the BOSS sample of quasars (Ross et al. 2013). In order to further check their suitability we compute the autocorrelation function of the simulated quasars, ξ_{qq} . We find that ξ_{qq} , while noisy as expected with not many objects, it has a shape that is approximately consistent with the CDM autocorrelation function appropriate for the simulation. We assign Poisson errors to the quasar autocorrelation function data points and carry out a fit of the bias factor, b_q relating the linear matter and quasar autocorrelation function over scales from $r = 4 h^{-1}$ Mpc to $r = 70 h^{-1}$ Mpc. We find $b_q = 4.1 \pm 0.8$, consistent at the 1σ level with the $b_q = 3.6$ (Font-Ribera et al. 2013) from the SDSS/BOSS quasar sample.

The simulation Ly α emission in the model is derived from the baryonic matter density field. We try two variations of the model:

Model G. The Ly α emission intensity is directly proportional to the matter density. This model represents Ly α emission uniformly tracing the large scale structure of the Universe (albeit in a biased fashion), for example being due to star forming galaxies. We have

$$\mu_{\text{Ly}\alpha}(x) = \langle \mu \rangle b_\alpha \rho(x), \quad (11)$$

where $\rho(x)$ is the baryonic matter density in units of the mean at a point separated by vector x from the coordinate origin.

Model Q. We assume that quasars are responsible for Ly α emission intensity with a Ly α surface brightness that is proportional to the product of the density and the inverse of the square of the distance from a quasar. We have for a given Ly α emission pixel,

$$\mu_{\text{Ly}\alpha}(x) = \mu_0 \rho \Gamma(x), \quad (12)$$

where $\Gamma(x)$ is the radiation intensity field computed in the optically thin limit, assuming all quasars have the same luminosity, L_0 , and r_i is the distance from the point in question to quasar i :

$$\Gamma(x) = \sum_{i=1}^{n_q} L_0 \frac{1}{r_i^2} e^{-r_s/r_i}. \quad (13)$$

Here the product $L_0 \mu_0$ is a constant, a free parameter which we set by fitting the amplitude of $\xi_{q\alpha}$ in the model to the observational data from SDSS/BOSS DR12. This model is meant to approximate scenarios where the energy from quasars is distributed to nearby gas following an inverse square law and induces Ly α emission. This could be through fluorescent emission e.g., Kolmeier et al.

(2010), hard quasar ionizing radiation heating the gas, or other mechanisms. The $e^{(-r/r_s)}$ term smooths the Ly α intensity field on small scales (we use $r_s = 2 h^{-1}$ Mpc). Without it, the small scale behaviour of $\xi_{q\alpha}$ is too steep. We leave investigation of the physics of the region within $2 h^{-1}$ Mpc of quasars to more sophisticated future simulations than our toy models.

In Figure 8 we show slices through the Ly α emission field in our two models. In each case, we have adjusted the mean Ly α surface brightness by tuning the parameters product $L_0 \mu_0$ in Equations 12 and 13 so that the quasar-Ly α emission cross-correlation function in the models is consistent with the results from SDSS DR12 (see next section). We can see that in the Model G case the emission does indeed trace structure, and prominent filaments can be seen. Looking at the Model Q panel, there is much more inhomogeneity in the emission. By design, the Ly α surface brightness close to quasars is similar to Model G, but in the regions far from quasars there are darker voids in the Ly α emission. The mean Ly α surface brightness is also lower in Model Q. We find $\langle \mu_\alpha \rangle = 1.5 \times 10^{-21} \text{ erg s}^{-1} \text{ cm}^{-2} \text{ arcsec}^{-2}$ for model G (assuming $b_\alpha = 3$), which is consistent with what was found from the linear theory model G in Section 3.1. For model Q, we find $\langle \mu_\alpha \rangle = 7.0 \times 10^{-22} \text{ erg s}^{-1} \text{ cm}^{-2} \text{ arcsec}^{-2}$. Although the $\langle \mu_\alpha \rangle$ values are only a factor of ~ 4 apart for model G and Q, we see below that the bias factor $b_\alpha = 3$ applicable only to model G strongly affects the clustering measures $\xi_{q\alpha}$ and $\xi_{q\alpha}$.

5.2 Quasar-Lyman-alpha emission cross-correlation in simulations

We next compute $\xi_{q\alpha}$ for the quasars and the model G and model Q Ly α emission fields in the simulation. First we move the quasars and emission field into redshift space. We use one axis of the simulation volume as the line of sight, moving quasars to their redshift space positions and convolving the Ly α emission field with the line-of-sight peculiar velocity field. We apply Equation 1 to the resulting quasar distribution and emission field, giving $\xi_{q\alpha}$ results which are shown in Figure 9. Because of the limited resolution of the simulation (we are working with sightlines spaced by $400/256 = 1.6 h^{-1}$ Mpc), there is no clustering information below $r = 2 h^{-1}$ Mpc.

We can see that $\xi_{q\alpha}$ for model G is approximately consistent with the linear theory model which was earlier (Section 3.1) found to be a reasonable fit to the observational data. This is expected, the simulation model was designed to be qualitatively the same, i.e. Ly α emission being a biased tracer of the mass distribution.

Looking at the results for model Q, we can see that the amplitude of $\xi_{q\alpha}$ is also similar to the observations (given the large error bars) and to model G. The lack of emission seen in the void regions in Figure 8 does not affect the fit, showing once more that only the emission with $\sim 15 h^{-1}$ Mpc of quasars is relevant to $\xi_{q\alpha}$.

In Figure 10, we show the projected quasar-Ly α emission cross-correlation function, $w_{q\alpha}$ for model Q, along with the SDSS data points and the larger scale of the quasar Ly α blob data from Figure 4. The simulation and observations are in reasonable agreement.

5.3 Forest-Lyman-alpha emission cross-correlation in simulations

We use the same simulations to compute $\xi_{f\alpha}$, again with the estimator of equation 8. The results are shown in Figure 11, where it can be seen that the Model G simulation curve follows the curve for

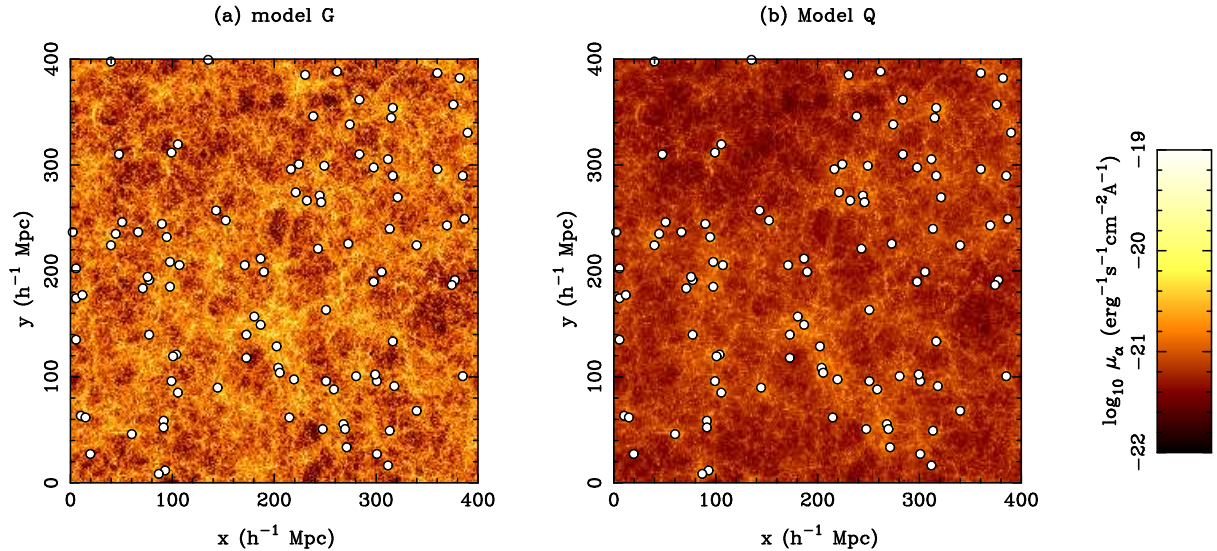


Figure 8. Slices ($40h^{-1}\text{Mpc} = 10\%$ of the box thick) through the simulation $\text{Ly}\alpha$ emission field in the two toy models model of Section 5.1. The $\text{Ly}\alpha$ emission surface brightness is shown by a colour scale and the positions of bright quasars by points. The quasar- $\text{Ly}\alpha$ emission cross-correlation function in both cases is consistent with the SDSS observations in this paper, but model G overpredicts the $\text{Ly}\alpha$ forest-emission cross-correlation by a factor of > 10 .

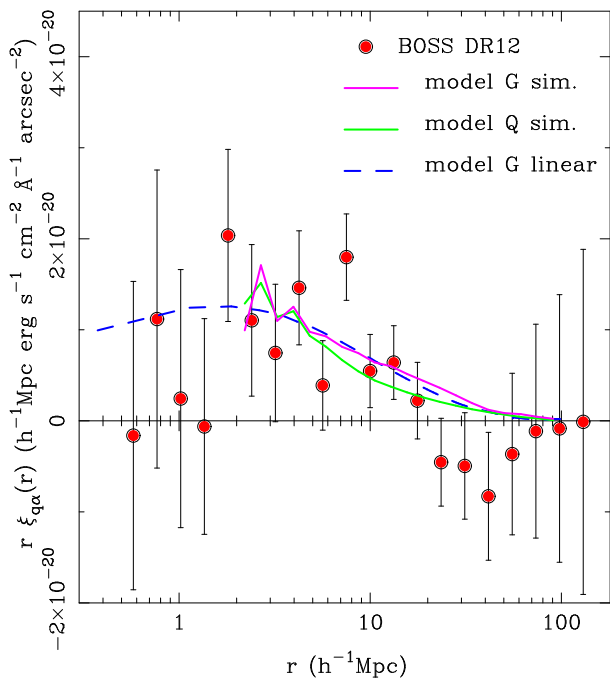


Figure 9. The quasar- $\text{Ly}\alpha$ emission cross-correlation function, in the simulation-based models G and Q, as well as the linear theory version of model G. The SDSS/BOSS data points are also shown.

the linear theory model G, although not as closely as for $\xi_{q\alpha}$ (Section 3.1). Both it and the linear theory curve are significantly larger in amplitude (while being negative in sign as expected because of the negative bias of the forest) than the observations. Model Q, on the other hand is much smaller in amplitude, reflecting the fact that most of the volume of space is far from quasars and therefore has little $\text{Ly}\alpha$ emission. The model Q results for $\xi_{q\alpha}$ and $\xi_{f\alpha}$ show that it is possible to realize a large-scale distribution of $\text{Ly}\alpha$ surface brightness which is consistent with both sets of observations. This was not trivial, as it could have been the case that both observations

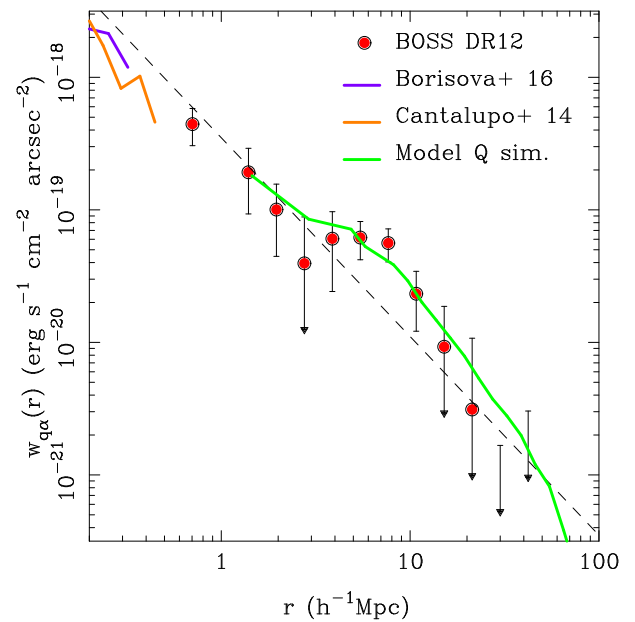


Figure 10. The projected quasar- $\text{Ly}\alpha$ emission cross-correlation function in the simulation of model G, together with the observational data points from Figure 4.

were mutually inconsistent, which would have meant that there was some problem with the measurement.

While we have shown that it is possible to distribute $\text{Ly}\alpha$ surface brightness in a way which matches observations (at least on scales $r > 2h^{-1}\text{Mpc}$), we have done this using a toy model. In future work that extends that of e.g., Kollmeier et al. (2010) and Kakiichi and Dijkstra (2017), it will be interesting to see if a first principles physical model is able to reproduce both the Borisova et al (2016) results and our observational data on large scales. Radiative transfer will be important to understand the $\text{Ly}\alpha$ emission, but it may also be relevant when considering the $\text{Ly}\alpha$ forest and $\xi_{f\alpha}$. For example, we

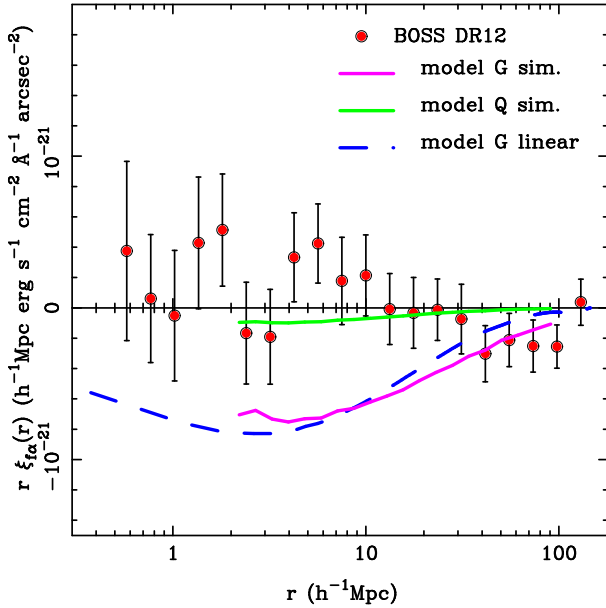


Figure 11. The forest- Ly α emission cross-correlation function in simulations (solid lines, purple for model G and green for model Q) and the SDSS DR12 observations (points with error bars). The dashed line shows the results for the linear theory version of model G.

have not included the quasar proximity effect (Bajtlik et al. 1988) in our modelling, which could suppress $\xi_{f\alpha}$.

6 SUMMARY AND DISCUSSION

6.1 Summary

We have searched for the signature of large-scale structure in the Ly α emission intensity of the Universe between redshifts $z = 2 - 3.5$, using cross-correlation techniques applied to data from SDSS/BOSS DR 12. Our findings are as follows:

(1) We have detected structure on scales from $1 - 15h^{-1}\text{Mpc}$ in the cross-correlation of quasars and Ly α emission, $\xi_{q\alpha}$. The shape of $\xi_{q\alpha}$ on these scales is consistent with the linear ΛCDM shape, as seen in our earlier work (C16). Improving on the earlier work, we have identified a source of light contamination not previously accounted for, due to the effect of quasar clustering on cross-fibre light. The amplitude we find is lower by 50% than in C16 because of this, but our conclusions with respect to $\xi_{q\alpha}$ are not qualitatively changed.

(2) We do not detect any signal when cross-correlating the Ly α forest flux in spectra with the Ly α emission samples (the relevant statistic is $\xi_{f\alpha}$). This non-detection allows us to place limits on the mean surface brightness of Ly α emission in a model where the emission traces the biased matter density field. The upper limit from this is $\langle\mu_{\alpha}\rangle < 1.2 \times 10^{-22} \text{ erg s}^{-1} \text{ cm}^{-2} \text{ arcsec}^{-2}$ at the 95% confidence level. The corresponding upper limit on the associated star formation rate density is $\rho_{\text{SFR}}(z = 2.55) < 0.01 \left(\frac{3}{b_{\alpha}}\right) M_{\odot} \text{ yr}^{-1} \text{ Mpc}^{-3}$. This is the same value as that measured from individually detected Ly α emitters.

(3) We have used cosmological hydrodynamic simulations to jointly examine $\xi_{q\alpha}$ and $\xi_{f\alpha}$ in toy models where Ly α emission traces either the large-scale structure in the star forming galaxy distribution (model G), or is associated more locally with quasars

(model Q). In model Q, we attenuate the Ly α surface brightness around quasars with an inverse square law, and as a result the 97% of the volume of space more than $15h^{-1}\text{Mpc}$ from a quasar has a very low level of Ly α emission. We find that only model Q can match the observational measurements of both $\xi_{q\alpha}$ and $\xi_{f\alpha}$.

(4) We have computed the projected Ly α surface brightness profiles around SDSS quasars by projecting our $\xi_{q\alpha}$ results into a pseudo narrow band. Extrapolating our results to small scales using a power law we find approximate consistency with the projected Ly α profiles measured on $< 0.5h^{-1}\text{Mpc}$ scales from the bright Ly α blobs seen around quasars by Cantalupo et al. 2014 and Borisova et al. 2016.

(5) Taken together, (1-4) above make it likely that the Ly α emission detected in $\xi_{q\alpha}$ is due to reprocessed energy from the quasars themselves and the Ly α emission from star forming galaxies is at a level not much different with that from individually detected Ly α emitters.

6.2 Discussion

In our previous work on the Ly α emission-quasar cross-correlation (C16) we explored possible interpretations for the signal. It was estimated that it is extremely unlikely that fluorescent emission due to quasar radiation is responsible, but that reprocessed HeII ionizing radiation from quasars or heating from quasar jets are both feasible on energetic grounds. The other prominent possible explanation was that the Ly α emission seen was due to escape of Ly α radiation from star forming galaxies. Converting the Ly α surface brightness into a mean star formation rate density gave a surprisingly high value, which was similar to the estimated total dust-corrected SFR density, and ~ 30 times higher than the SFR density of known Ly α emitters. Because of an additional correction for light contamination, our present results are lower by approximately a factor of two, but because of the uncertainty in the total SFR density this does not change the overall conclusions. In our current work, we have seen that such a scenario is inconsistent with another observable, the Ly α emission-Ly α forest cross-correlation, $\xi_{f\alpha}$ and this therefore seems to leave quasar emission as the source of the Ly α emission as the only possible astrophysical explanation.

The non-detection of $\xi_{f\alpha}$ can be used to place interesting limits on the Ly α emission from galaxies that trace the large-scale structure. We find a 95% upper limit, which is very close to the value from known Ly α emitters. This means that we should see their effects with other samples in the near future with this type of analysis. We note that in Equation 10 where this limit is given, the limit scales like $3/b_{\alpha}$. This means that if the luminosity weighted bias factor of Ly α emission is lower than 3, the limit is less restrictive. This is likely if the Ly α emission is primarily from Ly α emitters rather than all galaxies (e.g., the bias of measured by Gawiser et al. 2007 and Gauita et al. 2010 is closer to 1.8). Nevertheless, the fact that we are close to the individually detected value means that it is not possible for the known Ly α emitters to be surrounded by very extensive halos of low surface brightness Ly α emission or very faint Ly α emitting galaxies, at least not enough to increase the total Ly α luminosity density by a factor $\sim 2 - 3$. This constraint is close to the amount seen in extremely deep imaging of Ly α emitters by Steidel et al. (2011), Matsuda et al. (2012), and Momose et al. (2014)

We have removed light contamination from our measurements of Ly α intensity clustering, but it is still possible that some unidentified light contamination still exists. This is a general problem for intensity mapping approaches to studying large-scale structure, as well as light from interloper lines (Pullen et al. 2016) the effect if

which is mitigated by cross-correlation. Nevertheless, these kind of techniques, particularly cross-correlation with multiple tracers if some are available should be useful in eliminating systematic errors. Once a detection of $\xi_{f\alpha}$ is made, and it is consistent with measurements of other related statistics this would help significantly as a check on our result. The fact that the $\xi_{q\alpha}$ results from SDSS are quite similar to an extrapolation of from sub megaparsec scales of quasar Ly α blob profiles (e.g., Borisova et al 2016) is supportive of the measurement.

Nevertheless, we may be at the limit of what can be done with this kind of non-specialized dataset. We are using a set of fibre spectra which were not designed for IM, and we are severely limited by light contamination. In future IM work it should be a priority to design the dataset to minimize light contamination. Wide field integral field spectroscopy, such as that being carried out by the HETDEX (Hill et al. 2016) should easily detect the signal that we have seen, with much better control over systematic errors.

We leave theoretical considerations related to the Ly α emission from quasars which is likely responsible for the signal we have seen to future work. In C16, we saw that it is energetically possible for quasars to be involved, but the detailed mechanisms should be studied using physical modelling, such as with hydrodynamic simulations and radiative transfer. The toy models we have considered in this paper involve limited actual modelling of physical processes. There are also several physical effects which have not been included at all, for example the so called ‘‘proximity effect’’ (Bajtlik et al. 1998, Khrykin et al. 2017) in the Ly α forest surrounding quasars. We have also not considered the effect of stochasticity, as in our modeling the Ly α emission is deterministically related to the matter density.

Acknowledgments

RACC thanks Simon White for conversations which lead to work in this paper. RACC is supported by NASA ATP grant NNX17AK56G, NSF AST-1615940, and NSF AST-1614853.

Funding for SDSS-III has been provided by the Alfred P. Sloan Foundation, the Participating Institutions, the National Science Foundation, and the U.S. Department of Energy Office of Science. The SDSS-III web site is <http://www.sdss3.org/>.

SDSS-III is managed by the Astrophysical Research Consortium for the Participating Institutions of the SDSS-III Collaboration including the University of Arizona, the Brazilian Participation Group, Brookhaven National Laboratory, Carnegie Mellon University, University of Florida, the French Participation Group, the German Participation Group, Harvard University, the Instituto de Astrofísica de Canarias, the Michigan State/Notre Dame/JINA Participation Group, Johns Hopkins University, Lawrence Berkeley National Laboratory, Max Planck Institute for Astrophysics, Max Planck Institute for Extraterrestrial Physics, New Mexico State University, New York University, Ohio State University, Pennsylvania State University, University of Portsmouth, Princeton University, the Spanish Participation Group, University of Tokyo, University of Utah, Vanderbilt University, University of Virginia, University of Washington, and Yale University.

REFERENCES

Ahn, C., et al. 2014, *ApJS*, 211, 17
 Alam, S., 2015, *ApJS*, 219, 12

Albareti et al., 2017, *ApJS*, 233, 25
 Bajtlik, S., Duncan, R. C., Ostriker, J. P., 1988, *ApJ* 327, 570
 Bandura, K. et al., 2014, *Proc. SPIE Int. Soc. Opt. Eng.*, 9145:22, 2014. doi: 10.1117/12.2054950.
 Benitez, N., et al., 2014, *J-PAS Red Book*, arXiv:1403.5237
 Blanc, G.A., et al., 2011, 736, 31
 Bolton, A., et al. 2012, *AJ*, 144, 144
 Borisova, E., et al., 2016, *ApJ*, 831, 39
 Bouwens, R. J., et al. 2010, *ApJ*, 709, L133
 Bovy, J., et al. 2011, *ApJ*, 729, 141
 Busca, N. et al., 2013, *A & A*, 552, 96
 Cantalupo, S., Arrigoni-Battaia, F., Prochaska, J. X., Hennawi, J. F., & Madau, P. 2014, *Nature*, 506, 63
 Carilli, C.L., 2011, *ApJ Lett.*, 730, L30
 Cassata, P. et al. 2011, *Å*, 525, 143
 Castander, F.J., et al. 2012, *Proc. SPIE*, 8446, 6
 Chang, T.-C., Pen, U.-L., Bandura, K., and Peterson, J. B., 2010, *Nature*, 466, 463
 Cisewski, J., Croft, R.A.C., Freeman, P.E., Genovese, C.R., Khandai, N., Ozbek, M., and Wasserman, L., 2014, *MNRAS*, 440, 2599
 Dawson, K.S., et al., 2013, *AJ*, 145, 10
 Davis, M., Newman, J. A., Faber, S. M. & Phillips, A. C. 2001, in *Deep Fields* (eds Cristiani, S. Renzini, A. & Williams, R. E.) 241 (Springer)
 Delubac, T., et al. 2015, 574, 59
 Di Matteo, T., Khandai, N., DeGraf, C., Feng, Y., Croft, R. A. C., Lopez, J., and Springel, V., 2012, *ApJ*, 745, 29
 Doré et al. 2014, arXiv:1412.4872
 Eisenstein, D.J. et al. 2011, *Astronomical Journal* 142, 72
 Font-Ribera, A., et al. 2013, *JCAP*, 05, 018
 Font-Ribera, A. et al., 2014, *JCAP*, 05, 27
 Gallego, S.G. et al., 2018, *MNRAS*, 475, 3854
 Gawiser, E., et al. 2007, *ApJ*, 671, 278
 Gould, A., & Weinberg, D. H. 1996, *ApJ*, 468, 462
 Gronwall, C., et al., 2007, *ApJ*, 667, 79
 Guaita, L., et al. 2010, *ApJ*, 714, 255
 Gunn, J.E., et al. 1998, *AJ*, 116, 3040
 Gunn, J.E., et al. 2006, *AJ*, 131, 2332
 Hennawi, J. F., Prochaska, J. X., Cantalupo, S., & Arrigoni-Battaia, F. 2015, *Sci*, 348, 779
 Hernquist, L., Katz, N., Weinberg, D. H. and Miralda-Escudé, J., *ApJ*, 457, L51
 Hill, G.J. et al., 2016, *Proceeding of "Multi-Object Spectroscopy in the Next Decade"*, Eds. Skillen, I., Balcells, M., & Trager S., ASP Conference Series, Vol. 507. San Francisco: Astronomical Society of the Pacific, 2016, p.39
 Hogan, C. J., & Weymann, R. J. 1987, *MNRAS*, 225, 1
 Kaiser, N. 1987, *MNRAS*, 227, 1
 Kakiichi, K and Dijkstra, M., 2017, *MNRAS*, submitted, arXiv:1710.10053
 Keating, G.K., et al., (2015), *ApJ*, 814, 140
 Kirkpatrick, J.A., Schlegel, D.J., Ross, N.P., Meyers, A.D., Hennawi, J.F., Sheldon, E.S., Schneider, D.P., Weaver, B.A., 2011, *ApJ*, 743, 125
 Kollmeier, J. A., Zheng, Z., Davı, R., et al. 2010, *ApJ*, 708, 1048
 Kovetz, E.D., et al., 2017, *Physics Reports*, submitted, arXiv:1709.09066
 Khrykin, I. S., Hennawi, J. F. & McQuinn, M., 2017, *ApJ*, 838, 96
 Lee, K.G., et al. 2013, *AJ*, 145, 69
 Madau, P., Meiksin, A., & Rees, M.J., *ApJ* 475, 429 1997,
 Martin, D. C., Chang, D., Matuszewski, M., et al. 2014, *ApJ*, 786, 106
 Matsuda, Y., Yamada, T., Hayashino, T., et al. 2012, *MNRAS*, 425, 878
 McDonald, P., 2003, *ApJ*, 585, 34
 Momose, R., Ouchi, M., Nakajima, K., et al. 2014, *MNRAS*, 442, 110
 Noterdaeme, P, Petitjean, P., Ledoux, C., & Srianand, R., 2009, *A&A*, 505, 1087
 Noterdaeme, P. et al., 2012, *A&A*, 547, 1
 Ouchi, M., et al. 2008, *ApJS*, 176, 301
 Ozbek, M., and Croft, R.A.C., 2016. *MNRAS*, 456, 3610
 Paris, I. et al. 2012, *Å*, 548, 66
 Paris, I., et al., 2017, *A&A*, 597, 79
 Partridge, R.B. & Peebles, P.J.E., 1967, *ApJ*, 147, 868

Table 1. The fraction of light contaminating nearby fibres as a function of fibre separation on the CCD

Δ_{fibre}	f_{contam}
1	2×10^{-3}
2	6.5×10^{-4}
3	2×10^{-4}
4	2×10^{-4}

Peeples, M.S., Weinberg, D.H, Davé, R., Fardal, M., & Katz N., 2010, MNRAS401, 1281
 Pullen, A.R., Doré, O., and Bock, J., 2014, ApJ, 786, 111
 Pullen, A.R., Hirata, C., Doré, O. and Racanelli, A. 2016, PASJ, 68, 12
 Pullen, A.R., Serra, P., Chang, T.-C., Doré, O., and Ho, S. 2018, MNRAS, *tmp* 1181
 Ross, N.P., et al., 2013, ApJ, 773, 14
 Schlegel, D.J., Finkbeiner, D.P. & Davis, M., 1998, ApJ, 500, 525
 Silva, M., Santos, M., Gong, Y. And Cooray, A., 2013, ApJ, 763, 132
 Slosar, A., et al. 2013, JCAP, 04, 026
 Smee, S.A., et al. 2013, AJ, 126, 32
 Smith, A., Tsang, B.T.H., Bromm, V., & Milosavljević, Miloš
 Springel, V. and Hernquist L., 2003, MNRAS, 339, 289
 Springel, V. 2005, MNRAS, 364, 1105
 Steidel, C. C., Bogosavljević, M., Shapley, A. E., Kollmeier, J. A., Reddy, N. A., Erb, D. K. and Pettini, M. ApJ, 2011, 736, 160
 Wold, I. G. B., Finkelstein, S. L., Barger, A. J., Cowie, L. L. & Rosenwasser, B., ApJ 848, 108
 Yéche, C., et al., 2010, A&A, 523, 14
 Zheng, Z., Cen, R., Trac, H., Miralda-Escudé, J., 2010, ApJ, 716, 574
 Zheng, Z., Cen, R., Trac, H., Miralda-Escudé, J., 2011, ApJ, 726, 38

APPENDIX A: LIGHT CONTAMINATION

The light from all one thousand fibres in the spectrograph is dispersed onto the same 4096 column CCD. There is therefore the potential for light from one fibre to leak into the extraction aperture for another fibre. The data reduction pipeline (Bolton et al. 2012) has been designed so that this level of light contamination is negligible for almost all purposes. In carrying out IM with the LRG spectra, we are however operating beyond what the instrument was designed to do. In C16 it was shown that for a given galaxy, light from quasars within 4 fibres measurably contaminates the galaxy spectrum. The effect of the contamination is such that each pixel receives a small fraction of the light from the same wavelength pixel of the contaminating spectrum. In Table 1 we show how this fraction, f_{contam} depends on fibre separation, Δ_{fibre} .

In C16 the contamination was dealt with during the computation of the cross-correlation function of quasars and Ly α emission. Pairs of quasars and Ly α emission pixels with Δ_{fibre} equal to 5 or less were excluded from the computation. Unfortunately we have discovered in the present paper that this was not sufficient to remove all effects of contamination from $\xi_{q\alpha}$. This is because additional contamination enters at second order, due to quasar clustering, as follows. Suppose we exclude a particular quasar-pixel pair from the $\xi_{q\alpha}$ computation. Because quasars are strongly clustered, there is a chance that another quasar is near to the excluded one and light from that quasar is also contaminating the pixel. The likelihood of this contamination occurring will depend on the clustering strength of quasars. This possibility was ignored during the calculations in C16, but here we find that it should be dealt with if the cross-correlation results are to be reliable.

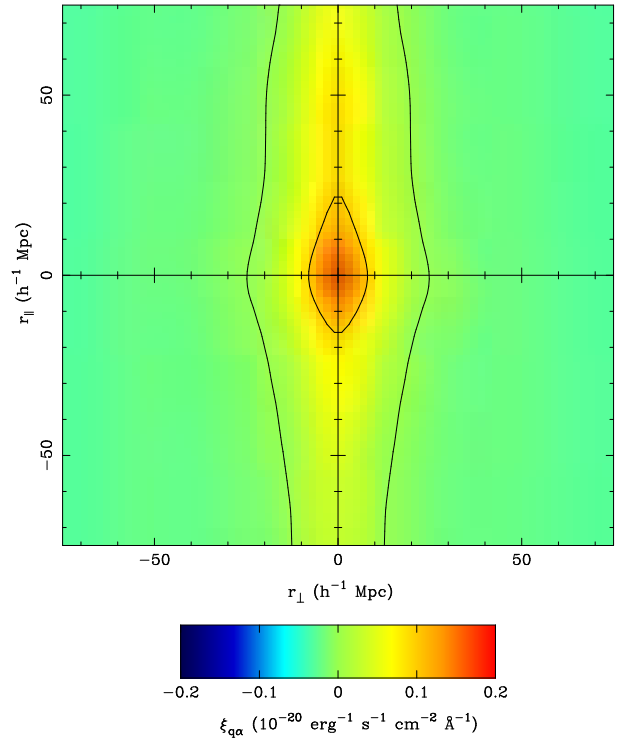


Figure 12. Light contamination: The cross-correlation function of quasars and Ly α emission, $\xi_{q\alpha}$ from mock spectra generated using light contamination only (see Section mockfibre).

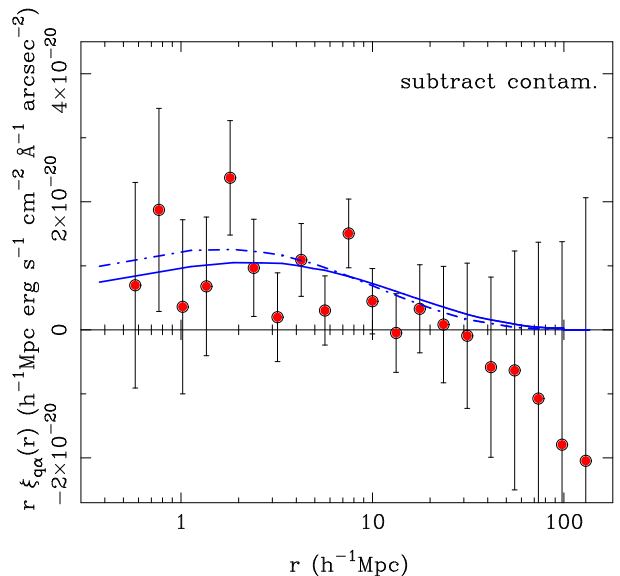


Figure 13. The cross-correlation function of quasars and Ly α emission, $\xi_{q\alpha}$. We have removed light contamination by using decontamination method (3) (see text): subtraction of $\xi_{q\alpha}$ computed from mock spectra generated using light contamination only (see Section 6.3).

6.3 Modelling contamination in $\xi_{q\alpha}$

We model the effects of light contamination on $\xi_{q\alpha}$ by making mock LRG fibre datasets which include only the light leakage from quasars, but not the light from the LRGs themselves. Measuring $\xi_{q\alpha}$ from these mock LRG spectra means that any $\xi_{q\alpha}$ signal seen will be from light contamination.

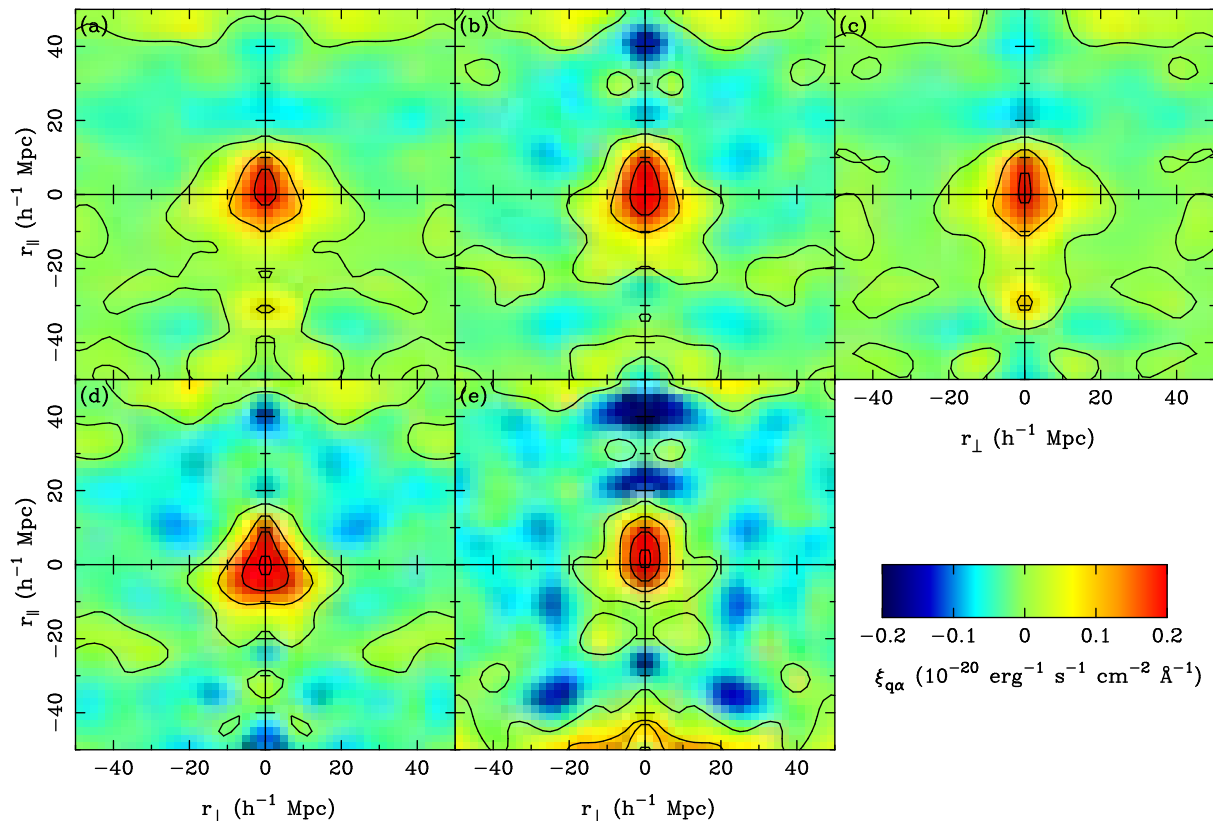


Figure 14. The quasar- $\text{Ly}\alpha$ emission cross-correlation function, $\xi_{q\alpha}(r)$ (see Equation 1) as a function of quasar-pixel separation across and along the line of sight. The different panels represent different ways of dealing with contamination or splitting the data. (a) The fiducial result (decontamination method 2), vetoing all pixels from the dataset which are within $\delta_{\text{fibre}} = 5$ and 75 mpc/h in the r_{\parallel} direction from a quasar. (b) All pixels in spectra within $\delta_{\text{fibre}} = 5$ of a quasar are excised from the dataset (decontamination method 1). (c) The contamination modeled in Section 6.3 is subtracted from the cross-correlation function (decontamination method 3). (d) Only pixels in spectra from the center of the field of view are used in the (otherwise fiducial) dataset. (e) Only pixels in spectra from the edge of the field of view are used in the (otherwise fiducial) dataset.

To make the mock datasets we use the information from Table 1. For each LRG fibre we find any quasars within $\Delta_{\text{fibre}} = 4$ or less, and then add a fraction of the light in a quasar spectrum (given in Table 1) to the LRG spectrum. We have tried two different approaches for doing this. In the first, we use the stacked mean quasar spectrum (taken from Section A2 in C16) as our contaminating light, using the same spectrum for every galaxy fibre. In the second case, we have used the actual SDSS quasar spectrum for the quasar in question as the contaminating light (again scaled appropriately). We find no significant difference in the $\xi_{q\alpha}$ results from the two methods. This is not the case however when looking at the $\text{Ly}\alpha$ forest- $\text{Ly}\alpha$ emission cross-correlation (Section 6.5), where the stacked spectrum does not exhibit the individual $\text{Ly}\alpha$ forest fluctuations which cause contamination.

Once the mock LRG spectra have been made, we compute $\xi_{q\alpha}$ from them (Equation 1, using $w_{ri} = 1$). When doing this, we exclude pairs of quasars and pixels separated by 5 fibres or less, so that any contamination signal seen will be due to quasar clustering. The results are shown in Figure 13, where we plot $\xi_{q\alpha}$ as a function of distance across and along the line of sight. We can see that the light contamination does result in a significant $\xi_{q\alpha}$ signal, with the influence stretching along the line of sight. Comparing Figure 13 to Figure 3 (which shows $\xi_{q\alpha}$ without contamination), we can see that the true signal is more centrally concentrated, dominating over the contamination, on scales $|r_{\perp}| < 10h^{-1}\text{Mpc}$ and $|r_{\parallel}| < 10h^{-1}\text{Mpc}$. The contamination is however substantial, reaching 50% of the

signal value even on these scales. It is therefore important to robustly remove it.

6.4 Removing contamination from $\xi_{q\alpha}$

We carry out removal of this extra light contamination using three different approaches. We test that they give consistent results for $\xi_{q\alpha}$ below.

(i) Decontamination method (1): Removal of all galaxy fibres within $\Delta_{\text{fibre}} = 5$ from the dataset. This is the most extreme solution—if any LRG fibre is within 5 fibres or less of a QSO fibre it is completely removed from the dataset. Unfortunately, the significant number of quasar fibres on each plate mean that the majority of galaxy fibres is removed in this method. Of 1570095 LRG fibres in the initial dataset, only 574603 (37 %) remain after culling. This greatly reduces the statistical power of the measurement.

(ii) Decontamination method (2): Similar to method (1), we remove contaminated LRG pixels from the dataset. However instead of removing an entire fibre if it is within $\delta_{\text{fibre}} = 5$ or less of a QSO, we excise data on a pixel by pixel basis. If the pixels are within the δ_{fibre} constraint we remove them, but only if they are also within $\pm 75h^{-1}\text{Mpc}$ in the line-of-sight direction of any quasar. This deals with contamination, but only 8.4 % of the pixels are removed. This decontamination method is our fiducial one, and was used to compute the results shown in Figure 1 and 3.

(iii) Decontamination method (3): We compute $\xi_{q\alpha}$ using the

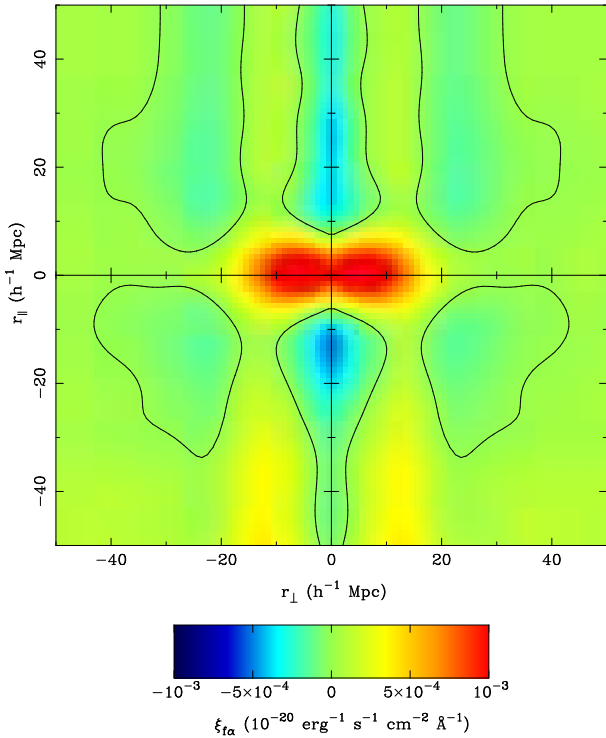


Figure 15. Light contamination: The cross-correlation function of Ly α emission and the Ly α forest, $\xi_{f\alpha}$ for spectra from BOSS DR12 (points with error bars). The actual signal predicted for $\xi_{f\alpha}$ in real data is negative (because the Ly α forest has negative bias).

entire dataset, except for quasar-pixel pairs within $\delta_{\text{fibre}} = 5$ (as was done in C16). We then subtract $\xi_{q\alpha}$ computed from contamination alone, using the mock LRG spectra of Section 6.3 (i.e. we subtract what is plotted in Figure 13).

In Figure 14, we show the $\xi_{q\alpha}$ results for BOSS DR12 after applying our decontamination methods (the three panels in the top row). Each of the panels is qualitatively similar which is not a trivial result, given the large differences in how the contamination is dealt with by the three methods. All panels exhibit Ly α emission centered on the origin, with similar amplitude, and with a hint of elongation in the line of sight direction. To determine the level of quantitative agreement, we fit the linear CDM model of Equation 2. The amplitude, $b_f b_\alpha f_\beta \langle \mu \rangle$ for method (1) is $b_q b_\alpha f_\beta \langle \mu \rangle = 1.21^{+0.49}_{-0.49} \times 10^{-20} \text{ erg s}^{-1} \text{ cm}^{-2} \text{ arcsec}^{-2}$, for method (2), $b_q b_\alpha f_\beta \langle \mu \rangle = 1.51^{+0.31}_{-0.29} \times 10^{-20} \text{ erg s}^{-1} \text{ cm}^{-2} \text{ arcsec}^{-2}$, and for method(3) is $b_q b_\alpha f_\beta \langle \mu \rangle = 1.45^{+0.29}_{-0.32} \times 10^{-20} \text{ erg s}^{-1} \text{ cm}^{-2} \text{ arcsec}^{-2}$. These amplitude results are all within one sigma of each other (as are the shape parameter Ω fits). These results give us confidence that the contamination due to quasar clustering identified above has been dealt with.

In C16, evidence was found that the fibres on the edge of the telescope field of view (where the camera image has lower optical quality) yield a smaller signal (by 2σ compared to the fiducial results in that paper) than those in the center of the field of view. We have repeated this test with the BOSS DR12 dataset with the $\xi_{q\alpha}$ results being shown in the bottom panel of Figure 14. One can see that the pattern in $r_{\parallel} - r_{\perp}$ space is similar to the upper panels. Although panel (e) (edge fibres) appears to have a large amplitude, the statistical error bar is also significantly larger (the large fluctuations seen away from the origin are also due to this). A fit to

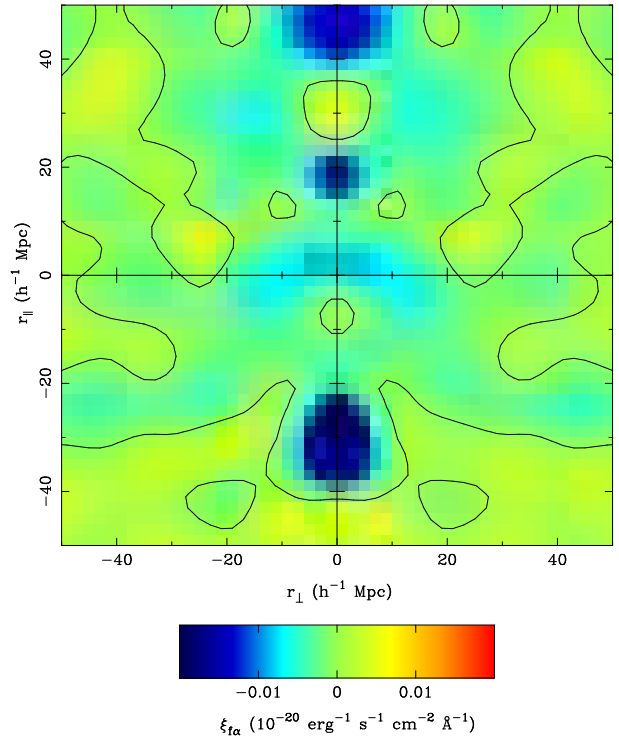


Figure 16. The cross-correlation function of Ly α emission and the Ly α forest, $\xi_{f\alpha}$ for spectra from BOSS DR12 (points with error bars) as a function of separation parallel to and perpendicular to the line of sight. We have eliminated all fibres within $\delta_{\text{fibre}} = \pm 5$ of a quasar before computing the cross-correlation. The predicted amplitude of $\xi_{f\alpha}$ is negative (because the Ly α forest has negative bias). The cross-correlation function plotted here is consistent with noise.

the CDM model for the center and edge fibres yields an amplitude of $b_q b_\alpha f_\beta \langle \mu \rangle = 1.22^{+0.36}_{-0.34} \times 10^{-20} \text{ erg s}^{-1} \text{ cm}^{-2} \text{ arcsec}^{-2}$, and $b_q b_\alpha f_\beta \langle \mu \rangle = 2.10^{+0.74}_{-0.70} \times 10^{-20} \text{ erg s}^{-1} \text{ cm}^{-2} \text{ arcsec}^{-2}$, respectively. This is consistent with what was seen in C16, that the reduction in optical quality at the edge of the field of view make a signal detection more statistically uncertain.

We have seen that the contamination induced by quasar clustering can be removed. It is of course possible that some other type of unidentified contamination is responsible for the remainder of what we see in the $\xi_{q\alpha}$ results. Two pieces of evidence supporting the fact that it is actual Ly α emission are the consistency with the extrapolation of results from smaller scales (Figure 4), and also consistency with a simple physical model which also explains the $\xi_{f\alpha}$ results (Section 5.1).

6.5 Modelling contamination in $\xi_{f\alpha}$

As quasar light contaminating galaxy fibres can yield a false $\xi_{q\alpha}$ signal, we check whether this also affects the Ly α forest-Ly α emission cross-correlation. We expect that in this case, the contaminating quasar light will contain the same Ly α forest fluctuations that are being cross-correlated against, and so this will yield a false signal. We model the contamination using our mock LRG fibre spectra datasets from Section 6.3. As mentioned above, we use the individual quasar spectra as contaminants rather than the stacked spectrum, in order that the Ly α forest fluctuations be present in the contamination. Results for $\xi_{f\alpha}$ from these mock spectra are shown in Figure 15. When comparing with the $\xi_{f\alpha}$ results from the DR12 data (Fig-

ure 7) it is important to realise that the color scales are very different (by a factor of 20 on the scale bar), and that the contamination seen in Figure 15 is quite small. It is nevertheless significant, however, and we can see that the cross-correlation of the negative bias Ly α forest fluctuations with the contaminating Ly α forest fluctuations (also with negative bias) in the mock Ly α emission spectra leads to a $\xi_{f\alpha}$ signal which is positive. This is the opposite sign to that expected from the genuine forest-emission correlation.

6.6 Removing contamination from $\xi_{f\alpha}$

The contamination can be dealt with in a similar fashion as for $\xi_{q\alpha}$. Unlike the case of cross-correlating with quasars, however, there is no easy way to apply method (2), because the objects to be cross-correlated with (the Ly α forest pixels) fill the spectrum (at least the interesting region where we are also looking for Ly α emission). We therefore use two of the three methods outlined in Section 6.4. Using Method (1) (excising whole fibres) again results in a much smaller dataset, and higher statistical noise in $\xi_{f\alpha}$. In Figure 16 we show the $\xi_{f\alpha}$ results using method (1). These can be compared to Figure 5 in the main text, which uses subtraction of contamination (method (3)). Figure 16 is noticeably noisier. Both methods yield a non-detection of any Ly α forest-emission cross-correlation.

We also try the edge/center test which was carried out with $\xi_{q\alpha}$. We find that for fibres at the edge of the field-of-view the amplitude of $\xi_{f\alpha}$ clustering is $b_f b_\alpha f_\beta \langle \mu \rangle = (-5.2 \pm 3.7) \times 10^{-22} \text{ erg s}^{-1} \text{ cm}^{-2} \text{ arcsec}^{-2}$. For fibres at the center we find $b_f b_\alpha f_\beta \langle \mu \rangle = -2.5^{+1.8}_{-2.9} \times 10^{-22} \text{ erg s}^{-1} \text{ cm}^{-2} \text{ arcsec}^{-2}$. Both are consistent with no measurable forest-emission correlation.